



## 25 **Summary**

26 Cooperation between receptors from the NLR superfamily is important for  
27 intracellular activation of immune responses. NLRs can function in pairs that, upon  
28 pathogen recognition, trigger hypersensitive cell death and stop pathogen invasion.  
29 Natural selection drives specialization of host immune receptors towards an optimal  
30 response, whilst keeping a tight regulation of immunity in the absence of pathogens.  
31 However, the molecular basis of co-adaptation and specialization between paired  
32 NLRs remains largely unknown. Here, we describe functional specialization in alleles  
33 of the rice NLR pair Pik that confers resistance to strains of the blast fungus  
34 *Magnaporthe oryzae* harbouring AVR-Pik effectors. We revealed that matching pairs of  
35 allelic Pik NLRs mount effective immune responses whereas mismatched pairs lead  
36 to autoimmune phenotypes, a hallmark of hybrid necrosis in both natural and  
37 domesticated plant populations. We further showed that allelic specialization is  
38 largely underpinned by a single amino acid polymorphism that determines  
39 preferential association between matching pairs of Pik NLRs. These results provide a  
40 framework for how functionally linked immune receptors undergo co-adaptation to  
41 provide an effective and regulated immune response against pathogens.  
42 Understanding the molecular constraints that shape paired NLR evolution has  
43 implications beyond plant immunity given that hybrid necrosis can drive  
44 reproductive isolation.

## 45 **Introduction**

46 Pathogens use an array of molecules, termed effectors, to successfully colonize hosts  
47 (Win et al., 2012). Intracellular detection of effectors relies on immune receptors from  
48 the nucleotide-binding, leucine-rich repeats (NLR) superfamily (Bentham et al., 2020;  
49 Jones et al., 2016; Saur et al., 2020). Upon recognition, NLRs act as nucleotide-operated  
50 switches, exchanging ADP for ATP (Bernoux et al., 2016; Tameling et al., 2002; Wang  
51 et al., 2019b; Williams et al., 2011), and oligomerise into supramolecular signalling  
52 platforms (Hu et al., 2015; Ma et al., 2020; Martin et al., 2020; Sharif et al., 2019;  
53 Tenthorey et al., 2017; Wang et al., 2019a; Zhang et al., 2015). This leads to immune  
54 responses, including programmed cell death, that restrict pathogen growth. The  
55 assembly of such sophisticated molecular machinery needs to be well coordinated and  
56 tightly regulated to ensure an efficient immune response, while avoiding the  
57 deleterious effect of constitutive immune activation (Chae et al., 2016; Karasov et al.,  
58 2017; Li et al., 2020; Richard and Takken, 2017).

59 NLRs form the most expanded and diversified protein family in plants (Meyers et al.,  
60 2003; Van de Weyer et al., 2019; Yue et al., 2012). Since their discovery, plant NLRs  
61 have been heavily studied and around 450 NLR proteins from 31 genera of flowering  
62 plants have been functionally validated (Kourelis et al., 2021). Plant NLRs present  
63 multiple layers of complexity (Barragan and Weigel, 2020), often functioning in  
64 genetically linked pairs (Eitas and Dangl, 2010; Griebel et al., 2014) or as part of  
65 complex immune networks (Wu et al., 2018). In such cases, NLRs specialize their role  
66 in immune activation, acting as “sensors” that detect pathogen effectors or as  
67 “helpers” that amplify and propagate immune signalling (Adachi et al., 2019b; Jubic  
68 et al., 2019). Paired NLRs are prevalent in plant genomes (Stein et al., 2018; Wang et  
69 al., 2019c) with a subset of sensor NLRs harbouring atypical domains integrated into  
70 their architecture (Bailey et al., 2018; Kourelis et al., 2021; Kroj et al., 2016; Sarris et al.,  
71 2016). These domains can be derived from pathogen host targets that act as sensor  
72 domains within NLRs by binding pathogen effectors (Bialas et al., 2018; Cesari et al.,  
73 2014a; Maidment et al., 2021; Oikawa et al., 2020).

74 Cooperating NLRs must balance a trade-off between adaptive evolution to fast  
75 evolving pathogens and maintaining a fine-tuned regulation of complex receptor  
76 assemblies. NLRs with different evolutionary trajectories may drift apart and  
77 eventually mismatch. When these mismatched NLRs are combined in the same  
78 individual through genetic crossing, constitutive immune activation can occur leading  
79 to deleterious phenotypes including dwarfism, necrosis, and lethality (Bomblies et al.,  
80 2007; Chae et al., 2014). These “Dangerous Mix” phenotypes are known in plant  
81 breeding as hybrid necrosis and have important implications in agriculture (Caldwell  
82 and Compton, 1943; Calvo-Baltanás et al., 2021; Hermsen, 1963a, b; Li and Weigel,  
83 2021; Wan et al., 2021; Yamamoto et al., 2010). In *Arabidopsis*, two genetically  
84 unlinked NLR proteins encoded on different chromosomes were shown to physically  
85 associate in the mixed immune background of hybrid plants, underpinning hybrid  
86 necrosis (Tran et al., 2017). Similarly, association between NLRs and alleles of non-  
87 NLR proteins derived from a different genetic background was also shown to induce  
88 NLR activation and autoimmune phenotypes (Barragan et al., 2019; Li et al., 2020).  
89 However, the biochemical basis of adaptive specialization in genetically linked NLR  
90 receptor pairs remains largely unknown. In particular, we know little about how  
91 coevolution between paired NLRs has impacted their activities. We lack a validated  
92 framework to explain how plant immune receptors adapt and specialize, even though  
93 this process has important consequences for plant diversification and evolution  
94 (Bomblies and Weigel, 2007; Calvo-Baltanás et al., 2021; Dobzhansky, 1937; Li and  
95 Weigel, 2021).

96 The rice NLRs *Pik-1* and *Pik-2* form a linked gene pair arranged in an inverted  
97 configuration on chromosome 11 with only ~2.5 Kb separating their start codons  
98 (Ashikawa et al., 2008). The *Pik* pair is present in the genetic pool of rice cultivars as  
99 two major haplotypes (Bialas et al., 2021; Kanzaki et al., 2012). *Pik* pairs belonging to  
100 the K haplotype confer resistance to strains of the rice blast fungus, *Magnaporthe oryzae*,  
101 that harbour the effector AVR-Pik (Ashikawa et al., 2008). The sensor NLR *Pik-1* binds  
102 AVR-Pik effectors through a heavy metal-associated (HMA) domain integrated into  
103 its architecture (De la Concepcion et al., 2018; Kanzaki et al., 2012; Maqbool et al.,  
104 2015). Upon effector recognition, *Pik-1* cooperates with the helper NLR *Pik-2* to

105 activate immune signalling (Zdrzalek et al., 2020) that leads to pathogen resistance.  
106 The Pik NLR pair occurs as allelic series in both Japonica and Indica rice cultivars  
107 (Chaipanya et al., 2017; Costanzo and Jia, 2010; Hua et al., 2012; Xu et al., 2008). The  
108 AVR-Pik effectors are also polymorphic and present signatures of selection (Bentham  
109 et al., 2021; Bialas et al., 2018; Yoshida et al., 2009). Allelic Pik NLRs have differential  
110 recognition specificities for the AVR-Pik variants (De la Concepcion et al., 2021;  
111 Kanzaki et al., 2012), which is underpinned by differential effector binding to the Pik-  
112 1 HMA domain (De la Concepcion et al., 2018; De la Concepcion et al., 2021; Maqbool  
113 et al., 2015). Two allelic variants of Pik-1, Pikp-1 and Pikm-1, acquired high-affinity  
114 binding to the *M. oryzae* AVR-Pik effector through convergent evolution of their HMA  
115 domains (Bialas et al., 2021). Additionally, Pikm-1 and Pikh-1 alleles have been shown  
116 to convergently evolve towards extended recognition specificity of AVR-Pik variants  
117 (De la Concepcion et al., 2021). This adaptive evolution towards recognition of rapidly  
118 evolving effectors has led to marked diversification of the integrated HMA domain  
119 (Bialas et al., 2021). As a consequence, Pik-1 HMA domain is the most sequence-  
120 diverged domain in the Pik NLR pair (Bialas et al., 2021; Bialas et al., 2018; Costanzo  
121 and Jia, 2010).

122 While Pik-1 acts as a sensor, Pik-2 acts as a helper NLR that is required for the  
123 activation of immune responses (Maqbool et al., 2015; Zdrzalek et al., 2020).  
124 Evolutionary analyses have shown that the genetic linkage of this NLR pair is ancient  
125 and revealed marked signatures of adaptive evolution in the integrated HMA domain  
126 of Pik-1 (Bialas et al., 2021). However, little is known about sensor/helper coevolution  
127 in Pik and how these multidomain proteins have adapted to changes in the rapidly  
128 evolving integrated HMA domain of Pik-1.

129 Here, we used two allelic variants of Pik, Pikp and Pikm, to explore NLR  
130 sensor/helper specificity (**Figure S1**). We challenged the hypothesis that throughout  
131 evolutionary time, these two allelic Pik pairs have become diverged and mismatched.  
132 Indeed, mismatched pairs of Pik-1 and Pik-2 display constitutive cell death  
133 reminiscent of autoimmune phenotypes. We identified a single amino acid  
134 polymorphism in the helper NLR Pik-2 that underpins both allelic specialization and

135 immune homeostasis. This finding allowed to reconstruct the evolutionary history of  
136 this coevolution. Altogether, these results demonstrate that NLR pairs can undergo  
137 co-adaptation and functional specialization, offering a molecular framework to  
138 understand how they evolve to respond to pathogen effectors while maintaining a  
139 tight regulation of immune responses.

## 140 **Results**

### 141 **A coevolved Pik NLR pair is required for efficient cell death response to AVR-Pik** 142 **effectors in *N. benthamiana*.**

143 Two of the most studied Pik alleles, Pikp (cv. K60) and Pikm (cv. Tsuyuake), fall into  
144 phylogenetically distinct groups (Bialas et al., 2021; De la Concepcion et al., 2021;  
145 Kanzaki et al., 2012). Pikm originated in the Chinese Japonica cultivar Hokushi Tami  
146 (Kiyosawa, 1978) while Pikp originated in the Indica cultivar Pusur in Pakistan  
147 (Kiyosawa, 1969). Thus, we hypothesised that these alleles have been exposed to  
148 differential selection pressures during domestication of elite cultivars and have  
149 undergone distinct evolutionary trajectories.

150 To test for sensor/helper specificity in allelic Pik pairs, we co-expressed the sensor  
151 NLR Pikm-1 with either the helper NLR Pikp-2 or Pikm-2 in *N. benthamiana* and  
152 assessed the capacity to trigger a cell death in response to rice blast effector variants  
153 AVR-Pik D, E or A (**Figure 1**). As previously reported, Pikm pair mediated a  
154 hierarchical cell death response in the order of AVR-PikD > AVR-PikE > AVR-PikA  
155 (De la Concepcion et al., 2018). However, the intensity of cell death was lower when  
156 Pikm-1 was co-expressed with Pikp-2 instead of Pikm-2 (**Figure 1, Figure S2**). Protein  
157 accumulation of both Pikp-2 and Pikm-2 proteins in planta was similar (**Figure S3**).

158 These results indicate that Pikm-2 is required for the full Pikm mediated cell death  
159 response to the AVR-Pik effectors in *N. benthamiana*. This suggests a possible  
160 functional specialization of the helper NLR Pik-2 towards an effective cell death  
161 response to these rice blast effectors.

### 162 **A single amino acid polymorphism in Pik-2 has an important role in cell death** 163 **responses to the AVR-Pik effectors.**

164 To dissect the basis of the differential cell death phenotypes displayed by Pikp-2 and  
165 Pikm-2 in response to the AVR-Pik effectors, we used site-directed mutagenesis to  
166 exchange the residues at each of the three Pik-2 polymorphic positions (**Figure S3**).  
167 We then co-expressed Pikm-1 and each of the Pik-2 mutants with either AVR-PikD,  
168 AVR-PikE or AVR-PikA. For each assay, we scored the cell death responses and

169 compared the differences with the Pikm control to qualitatively measure the  
170 contribution of each polymorphism to cell death (**Figure 2, Figure S4, S5, S6, S7**). In  
171 brief, this assay aimed to identify reciprocal mutations in Pikm-2 and Pikp-2 that may  
172 reduce or increase immune responses, when compared with wild-type Pikm-2.

173 A single amino acid change at position 230 was responsible for the major differences  
174 in cell death responses (**Figure 2**). Despite the similar properties of their side chains,  
175 the Asp230Glu mutation in Pikp-2 showed an increase in the level of cell death  
176 response to AVR-Pik effectors (**Figure 2A, S4A**). By contrast, the Glu230Asp mutation  
177 in Pikm-2 reduced the cell death response to each AVR-Pik effector compared with  
178 wild-type Pikm-2, displaying only a slight response to AVR-PikD (**Figure 2B, S4B**).  
179 This points to a major involvement of the Pikm-2 Glu230 residue in the extended  
180 response to AVR-Pik effectors observed in Pikm (De la Concepcion et al., 2018).

181 Mutations at polymorphic positions 434 and 627 did not have the strong effect  
182 observed in the mutants at position 230. The Thr434Ser and Met627Val mutations in  
183 Pikp-2 did not yield higher levels of cell death response compared with Pikm-2  
184 (**Figure S5A, C, S6A, C, S7A, C**). Likewise, neither Pikm-2 Ser434Thr nor Pikm-2  
185 Val627Met showed a lower level of cell death response compared with wild-type  
186 Pikm-2 (**Figure S5B, D, S6B, D, S7B, D**). Interestingly, Val627Met in Pikm-2  
187 consistently increased cell death responses, particularly to AVR-PikE and AVR-PikA  
188 (**Figure S5D, S6D, S7**) implying a negative contribution of Pikm-2 polymorphism  
189 Val627 towards cell death responses. All mutants had a similar level of protein  
190 accumulation in *N. benthamiana* compared to wild-type Pikp-2 and Pikm-2 (**Figure S3**).

191 Altogether, these results demonstrate that polymorphisms in Pik-2 play an important  
192 role in facilitating response to different AVR-Pik alleles. Particularly, a single  
193 polymorphic residue, Glu230, was revealed as a major determinant of the increased  
194 cell death responses to the AVR-Pik effectors displayed by the Pikm NLR pair.

195 **Mismatched Pik pair Pikp-1/Pikm-2 triggers constitutive cell death responses in *N.***  
196 ***benthamiana*.**



197 When independently evolved NLR receptors meet in the mixed immune background  
198 of a hybrid plant, it can lead to misregulation in the form of suppression (Hurni et al.,  
199 2014; Stirnweis et al., 2014) or constitutive activation of immune responses (Chae et  
200 al., 2014; Li et al., 2020; Tran et al., 2017).

201 The Pikp and Pikm allelic pairs trigger a strong cell death response in *N. benthamiana*  
202 when co-expressed with rice blast effector AVR-PikD, but not in the absence of effector  
203 (De la Concepcion et al., 2018; Maqbool et al., 2015). However, we noticed that when  
204 Pikp-1 was co-expressed together with Pikm-2, it led to cell death response in the  
205 absence of AVR-PikD (**Figure 3**). We did not observe NLR autoactivation in the  
206 reciprocal mismatched pair Pikm-1/Pikp-2 (**Figure 3**).

207 These results reveal signatures of coevolution in the Pikp and Pikm allelic pairs. We  
208 hypothesise that these allelic pairs have coevolved with their respective partners and  
209 have drifted enough to trigger a misregulated form of immune response when they  
210 are mismatched, leading to constitutive cell death in *N. benthamiana*.

### 211 **Pik autoactivity is linked to immune signalling.**

212 We sought to gain knowledge on the constitutive cell death mediated by Pikm-2 and  
213 understand the link with NLR activation. To this end, we mutated Pikm-2 in the  
214 conserved P-loop and MHD motifs and tested their ability to trigger constitutive cell  
215 death responses in the absence of the AVR-PikD effector.

216 The P-loop motif is conserved in NLR proteins and mediates nucleotide binding  
217 linked with oligomerization and NLR activation (Ma et al., 2020; Wang et al., 2019b).  
218 Loss-of-function mutations at this position render NLRs inactive and have been  
219 extensively documented (Tameling et al., 2002; Tameling et al., 2006; Williams et al.,  
220 2011). A Lys217Arg mutation in the P-loop motif of Pikp-2 abrogates Pik-mediated  
221 cell death responses to AVR-PikD in *N. benthamiana* (Zdrzalek et al., 2020). Introducing  
222 this mutation in Pikm-2 abolished Pikm-mediated cell death response to the rice blast  
223 effector AVR-PikD (**Figure 4**) and also abrogated the constitutive cell death response  
224 triggered by the Pikp-1/Pikm-2 NLR mismatch (**Figure 4**).

225 NLR activities are also altered by mutations in the MHD motif. An Asp to Val  
226 mutation in this motif is predicted to change ATP/ADP binding preference and, in  
227 many cases, renders NLRs constitutively active (Bernoux et al., 2016; Tameling et al.,  
228 2006; Williams et al., 2011). Contrary to other NLRs, introducing Asp559Val in the  
229 MHD motif of Pikp-2 abolished cell death responses to AVR-PikD (Zdrzalek et al.,  
230 2020). Consequently, we introduced the equivalent mutation in Pikm-2 and verified  
231 that it also abrogated cell death in autoimmune combinations (**Figure 4**), confirming  
232 that Pikm-2 requires an intact MHD motif to trigger cell death and strengthening the  
233 link between constitutive cell death and immune activation.

234 **NLR specialization and autoimmunity are linked to the same amino acid**  
235 **polymorphism.**

236 Interestingly, only mismatches involving Pikm-2 triggered cell death in the absence of  
237 the effector (**Figure 3**), suggesting that this NLR harbours the determinants of this  
238 autoactive phenotype. To understand the basis of Pikm-2-mediated autoimmunity,  
239 we used the point mutants in Pik-2 polymorphic positions presented above (**Figure**  
240 **S3**) to explore the determinant of constitutive cell death. To this end, we co-expressed  
241 each mutant with either Pikp-1 or Pikm-1 in the presence or absence of AVR-PikD  
242 effector (**Figure 5, Figure S8**). In this assay, we added AVR-PikD effectors as a positive  
243 control for cell death.

244 The Asp230Glu mutation in Pikp-2 conferred a strong cell death response in the  
245 absence of the effector when co-expressed with Pikp-1, while only residual  
246 constitutive activation could also be observed with Pikm-1 (**Figure 5**). By contrast, the  
247 reciprocal mutation at the equivalent position in Pikm-2 abrogated constitutive cell  
248 death in the presence of Pikp-1 and reduced the cell death response mediated by AVR-  
249 PikD recognition (**Figure 5**). Single mutations in any of the other polymorphic  
250 positions had no effect on constitutive cell death activation (**Figure S8**).

251 Additionally, we confirmed that constitutive cell death triggered by Pik-2 Asp230Glu  
252 is also dependent on the P-loop and MHD motifs, confirming that this mutation leads  
253 to immune activation (**Figure S9**). Interestingly, cell death responses were reduced but  
254 not completely abolished when Pikm-2 or Pikp-2 Asp230Glu were co-expressed with

255 a P-loop mutant of Pikp-1 (**Figure S10**). Protein accumulation of the Pikp-1 P-loop  
256 mutant and the Pik-2 P-loop and MHD mutants were equivalent to their wild-type  
257 counterparts (**Figure S11**). This unequal contribution of the P-loop motifs of sensor  
258 and helper NLRs adds an extra layer of information to the cooperation model of NLR  
259 activation previously proposed for Pik (Bialas et al., 2018).

260 Overall, we narrowed down a determinant of autoimmunity in the mismatched Pik  
261 pairs to a single amino acid polymorphism. Furthermore, we confirmed that this  
262 polymorphism mediates cell death phenotypes by a mechanism dependent on the P-  
263 loop and MHD motifs. Interestingly, the same polymorphism is related to the stronger  
264 cell death responses to AVR-Pik effectors mediated by Pikm (**Figure 2**). Altogether,  
265 this establishes a link between immune specialization and gain of constitutive cell  
266 death responses in NLR pairs, two hallmarks of coevolution.

### 267 **The Glu230 amino acid polymorphism has evolved in modern rice.**

268 Having identified a determinant of Pik NLR pair specialization and compatibility as  
269 a single amino acid polymorphism, we aimed to gain an evolutionary perspective of  
270 the specialization process of Pik-2. For this, we combined the Pik-2 coding sequences  
271 from rice cultivars described above with the Pik-2 orthologs from wild Asian and  
272 African relative species (Bialas et al., 2021; Stein et al., 2018) (see methods for accession  
273 numbers) and calculated the maximum likelihood phylogenetic tree rooted in the  
274 African outgroup species *Leersia perrieri* (**Figure 6A**).

275 Pik-2 sequences from wild rice species are phylogenetically distinct from those  
276 belonging to modern rice, with the exception of Nipponbare and Toto (**Figure 6A**).  
277 These modern varieties make two distinct groups harbouring Pikp cultivar K60 or  
278 Pikm cultivar Tsuyuake (**Figure 6A**) (Bialas et al., 2021; De la Concepcion et al., 2021).

279 To learn more of the evolutionary trajectory of Pik-2, we inferred the ancestral state of  
280 the nucleotide sequences coding for the polymorphic position 230. This analysis  
281 revealed that a Gly residue encoded by GGT is an ancestral state at this position and  
282 is still present in most Pik-2 sequences from wild *Oryza* species (**Figure 6A**).

283 A transition from GGT (coding for Gly) to GAT (coding for Asp) in position 230  
284 occurred before the split of *Oryza sativa* and *Oryza punctata* and has been maintained  
285 in Pik-2 NLRs of modern rice varieties clustering in the with the Pikp cultivar K60  
286 **(Figure 6A)**. This change opened the possibility of a non-synonymous Asp to Glu  
287 mutation by a GAT to GAA transversion, which occurred in the rise of the clade  
288 containing the Pikm cultivar Tsuyuake. This Asp230Glu polymorphism represents a  
289 specialization determinant in the Pikm NLR pair and ultimately rendered Pikm-2  
290 incompatible with Pikp-1.

291 To experimentally validate the reconstructed evolutionary history of Pik-2  
292 polymorphic position 230, we reverted this position in Pikm-2 to the ancestral state by  
293 introducing a Glu230Gly mutation and tested its ability to trigger cell death in *N.*  
294 *benthamiana*. The Glu230Gly mutation abolished the constitutive cell death triggered  
295 by Pikm-2 when co-expressed with Pikp-1 in the absence of the effector **(Figure 6B)**.  
296 This mutation did not abrogate the cell death response to the AVR-PikD effector,  
297 although it slightly reduced it compared with the wild type **(Figure 6B, Figure S12)**.  
298 Protein accumulation of Pikm-2 Glu230Gly was equivalent to wild-type Pikp-2 and  
299 Pikm-2 **(Figure S13)**.

300 Overall, having reconstructed the evolutionary history of Pik NLR specialization we  
301 propose a model where a multi-step mutation led to the emergence of Glu230  
302 polymorphism, which is linked to an efficient cell death response to AVR-Pik effectors  
303 in the Pikm pair. We further demonstrated that the rise of this polymorphism is  
304 associated with NLR incompatibility with mismatched sensor NLRs from the Pikp-  
305 like clade, triggering constitutive immune activation and cell death in the absence of  
306 pathogen effectors.

### 307 **Sensor/helper hetero-pairing alters protein accumulation in Pik NLRs.**

308 We aimed to obtain mechanistic understanding of Pik NLR pair coevolution and  
309 autoactivation. For this, we investigated whether accumulation of sensor Pik-1 or  
310 helper Pik-2 proteins is altered in the presence of the coevolved or mismatched pair.

311 After co-expression of both Pikp-1 and Pikm-1 alleles in *N. benthamiana* in combination  
312 with the helper Pikp-2 or Pikm-2 alleles followed by western blot, we observed that  
313 protein accumulation of Pik-1 and Pik-2 alleles were consistently increased when they  
314 were expressed together compared to co-expression with empty vector (**Figure 7A**).  
315 This is consistent with a model where Pik-1 and Pik-2 associate in sensor/helper NLR  
316 heterocomplexes, stabilizing both proteins (Zdrzalek et al., 2020).

317 Interestingly, accumulation of the helper Pik-2 in the autoimmune pair Pikp-1/Pikm-  
318 2 was consistently higher (**Figure 7A**). This could be due to a different sensor/helper  
319 stoichiometry in the constitutively active Pik complex, as observed in some activated  
320 NLR complexes (Hu et al., 2015; Sharif et al., 2019; Tenthorey et al., 2017; Zhang et al.,  
321 2015). This is also consistent with the finding that CC domain of Pik-2 NLR has the  
322 consensus MADA motif first identified in ZAR1 (Adachi et al., 2019a), indicating the  
323 possibility that Pik activation may involve oligomerization of multiple Pik-2 receptors  
324 as in the ZAR1 resistosome (Wang et al., 2019a).

### 325 **Coevolved and mismatched Pik pairs form heterocomplexes.**

326 Prompted by the differences in protein accumulation observed between different  
327 combinations of Pik-1 and Pik-2, we investigated whether cell death phenotypes in  
328 mismatched Pik pairs are underpinned by differences in NLR hetero-association.

329 We co-expressed C-terminally tagged Pikp-1 or Pikm-1 with either C-terminally  
330 tagged Pikp-2 or Pikm-2 in *N. benthamiana*. Following total protein extraction, we  
331 performed co-immunoprecipitation to test for differences in NLR association (**Figure**  
332 **7B**). Pikp-1 and Pikm-1 were also co-infiltrated with the rice NLR Pia-2 (the sensor  
333 NLR, also known as RGA5, of the immune receptor pair Pia) as a negative control.

334 Both Pikp-2 and Pikm-2 could be detected after immunoprecipitation of either Pikp-1  
335 or Pikm-1 sensor NLRs (**Figure 7B**). Additionally, none of the Pik-2 mutations  
336 generated above seem to have a measurable effect on the sensor/helper association  
337 (**Figure S14, S15**).

338 These results indicate that cell death phenotypes observed in mismatched pairs are  
339 not underpinned by major alterations in association. Instead, Pik sensor and helper

340 NLRs may form pre-activation complexes in the resting state and subtle changes,  
341 perhaps both in association and stoichiometry between Pik NLRs, govern cell death  
342 responses and autoimmune phenotypes described above.

343 **Sensor/helper association of Pik NLR pairs is independent of NLR activation.**

344 As Pik NLR pairs associate in pre-activation complexes (**Figure 7B**) (Zdrzalek et al.,  
345 2020), we investigated whether this process requires functional NLRs. We co-  
346 expressed the Pikm-2 P-loop and MHD mutants with either Pikp-1 or Pikm-1 in *N.*  
347 *benthamiana*. Following protein extraction and immunoprecipitation of Pik-1, we  
348 found that these mutations do not affect the ability to associate with the sensor NLR  
349 Pik-1 compared to wild-type Pikm-2 (**Figure 8**), although they completely abolish Pik-  
350 mediated cell death. Similarly, the reduced cell death activity in the Pik-1 P-loop  
351 mutant did not correlate with alterations in the association to the helper NLR Pik-2  
352 (**Figure S16**).

353 These results imply that pre-activated Pik NLR pair association does not require  
354 functional NLRs and is independent of nucleotide binding. In the native state such  
355 pre-activation complexes may require ADP/ATP exchange to induce or stabilise  
356 changes in receptor conformation and/or stoichiometry to trigger immune signalling.

357 **Sensor and helper Pik NLRs preferentially associate with their coevolved pair.**

358 To gain a deeper knowledge of Pik pair association, we investigated whether allelic  
359 Pik NLRs display any preference in association to their coevolved NLR pair. As both  
360 autoactive and non-autoactive pairs associate, we designed an NLR competition assay  
361 with a cell death readout to test for preferential association between allelic NLRs  
362 (**Figure S17**). For this, we took advantage of the constitutive cell death phenotype  
363 triggered by the association of Pikp-1 and Pikm-2 (**Figure S17A**). In a scenario where  
364 a non-autoactive Pik-2 NLR displays higher helper/sensor association to Pikp-1,  
365 Pikm-2 would be outcompeted from complex formation, reducing the levels of  
366 constitutive cell death (**Figure S17B**).

367 To test this, we transiently co-expressed both Pikp-1 and Pikm-2 NLRs in *N.*  
368 *benthamiana* using a fixed concentration (OD<sub>600</sub> 0.4) of *Agrobacterium tumefaciens* to

369 deliver each construct. We also co-delivered increasing concentrations of P<sub>ikp</sub>-2  
370 (spanning an OD<sub>600</sub> of 0–0.6) and scored the cell death phenotype (**Figure 9**).

371 Interestingly, P<sub>ikp</sub>-2 acted as a suppressor of autoimmune phenotypes triggered by  
372 P<sub>ikp</sub>-1/P<sub>ikm</sub>-2 as increasing concentrations of P<sub>ikp</sub>-2 lowered the constitutive cell  
373 death phenotype (**Figure 9A, B**). This reduction in cell death was evident even in the  
374 lowest concentration of P<sub>ikp</sub>-2 (**Figure 9A, B**), suggesting that P<sub>ikp</sub>-1 displays  
375 preference to signal through coevolved P<sub>ikp</sub>-2 rather than P<sub>ikm</sub>-2.

376 We also replicated this experiment co-infiltrating a fixed concentration of P<sub>ikp</sub>-1 and  
377 P<sub>ikp</sub>-2, with increasing concentration of P<sub>ikm</sub>-2. In agreement with a signalling  
378 preference between P<sub>ikp</sub>-1 and P<sub>ikp</sub>-2, P<sub>ikm</sub>-2 could not overcome the suppression  
379 by the presence of P<sub>ikp</sub>-2, even at the highest concentration (**Figure S18**).

380 To investigate whether the decrease in cell death is correlating with reduced  
381 association of the maladapted pair P<sub>ikp</sub>-1/P<sub>ikm</sub>-2 in the presence of P<sub>ikp</sub>-2, we  
382 immunoprecipitated P<sub>ikp</sub>-1 and tested for the presence of P<sub>ikp</sub>-2 or P<sub>ikm</sub>-2 (**Figure**  
383 **9C**).

384 Differences in protein accumulation observed in the different sensor/helper  
385 combinations of P<sub>ik</sub> pairs makes it particularly challenging to obtain even inputs for  
386 this experiment. As reported above (**Figure 7A**), the P<sub>ik</sub>-2 proteins are more stable in  
387 association with P<sub>ik</sub>-1, therefore, if a P<sub>ik</sub>-2 protein is outcompeted from a hypothetical  
388 complex, it will present reduced accumulation in the input. The contrary effect occurs  
389 in the P<sub>ik</sub>-2 proteins forming autoactive complexes, as they showed increased  
390 accumulation in autoactive combinations (**Figure 7A**), the amount of protein in  
391 concentrations where P<sub>ikp</sub>-2 supresses constitutive cell death may seem lowered.

392 Nevertheless, co-immunoprecipitation results depicted a preference in association of  
393 P<sub>ikp</sub>-1 to P<sub>ikp</sub>-2 over P<sub>ikm</sub>-2. Increasing concentrations of P<sub>ikp</sub>-2 reduced the  
394 association of P<sub>ikp</sub>-1 to P<sub>ikm</sub>-2, outcompeting P<sub>ikm</sub>-2 from a heterocomplex with  
395 P<sub>ikp</sub>-1 (**Figure 9C**). This correlates with the reduction of the constitutive cell death  
396 assay observed in the NLR competition experiments (**Figure 9A, B**).

397 Altogether, these data reveal that coevolved Pik NLRs display preference in  
398 association over non-coevolved NLRs. This represents another example of NLR pair  
399 co-adaptation. These differences may underpin the observed cell death phenotypes in  
400 response to effectors and in autoimmunity.

#### 401 **Pik helper/sensor association preference is underpinned by Pik-2 polymorphism.**

402 To shed light on the basis of the preferential binding between Pkp-1 and Pkp-2, we  
403 tested the role of the polymorphism 230 in this phenotype. For this, we repeated the  
404 NLR competition assay co-infiltrating a fixed concentration (OD<sub>600</sub> 0.4) of Pkp-1 and  
405 the autoactive mutant Pkp-2 Asp230Glu, with increasing amounts of Pkp-2.

406 The combination of Pkp-1 and Pkp-2 Asp230Glu led to a strong cell death in the  
407 absence of effector (**Figure 5**). However, increasing concentrations of Pkp-2  
408 significantly reduced this phenotype (**Figure 10**).

409 This indicates the Pik-2 Glu230 polymorphism may also be related to the preferential  
410 association between sensor and helper NLRs in addition to its role in specialization  
411 towards AVR-Pik effector response and autoimmunity.

#### 412 **Pik pair preferential association requires NLR activation.**

413 To investigate if the preferential sensor/helper association is related to the activation  
414 of the helper NLR Pkp-2, we tested whether the constitutive cell death mediated by  
415 Pkp-2 Asp230Glu could be suppressed by mutants that render Pkp-2 inactive.

416 Although Pik NLRs do not require a functional P-loop or MHD motif to form  
417 heterocomplexes (**Figure 8**), we did not observe reduction of cell death phenotypes  
418 with increasing concentrations of Pkp-2 mutants in the P-loop (Lys217Arg) or MHD  
419 (Asp559Val) motifs (**Figure 11**), even at the highest concentration. This indicates that  
420 the P-loop and MHD motifs are required for the preferential sensor/helper association  
421 observed in Pkp-1 and Pkp-2.

422 Altogether, these results suggest that changes in Pik sensor and helper NLR  
423 association from a resting state into an activated complex requires functional NLRs.  
424 This is consistent with studies in the Arabidopsis NLR RPP7, where a P-loop mutant



425 retains the ability to associate with autoactive forms of its incompatibility partner HR4  
426 but is not capable of forming higher order assemblies (Li et al., 2020).

## 427 **Discussion**

428 The work presented here highlights sensor/helper coevolution in an allelic rice NLR  
429 pair and the basis of their functional diversification towards differential effector  
430 recognition specificities (**Figure 12**). We discovered that a single amino acid  
431 polymorphism underpins specialization of the helper Pik-2 NLR to its corresponding  
432 Pik-1 sensor NLR. Changes in this residue affect cell death outcomes in effector  
433 recognition and autoimmune phenotypes. By narrowing down the contribution of  
434 NLR specialization to a single amino acid, we could trace the evolutionary history of  
435 this polymorphism (**Figure 12**).

436 The notion that NLRs can work together in pairs is now well-established in the field  
437 of plant-microbe interactions (Adachi et al., 2019b; Jubic et al., 2019). Under this  
438 emerging framework, it is predicted that cooperating NLRs co-adapt to optimise and  
439 maintain a tight control over immune responses. However, the extent to which paired  
440 NLRs coevolve to efficiently respond to pathogen effectors while keeping a fine-tuned  
441 regulation of immune responses is not well understood at the molecular level.  
442 Particularly intriguing is how rapid changes driven by coevolution with pathogen  
443 effectors and major evolutionary events, such as the integration of an unconventional  
444 domain, impact NLR co-adaptation.

445 The genetic linkage of the Pik NLR pair has been maintained in grass genomes for tens  
446 of millions of years and emerged before the integration of the HMA domain in Pik-1  
447 (Bialas et al., 2021). This suggests that Pik-1 and Pik-2 have been coevolving for a long  
448 time, potentially before providing resistance to the blast fungus. Thus, the integration  
449 of the HMA domain in Pik-1, and its subsequent rapid coevolution with rice blast  
450 effectors, may have represented a major perturbation on the coevolutionary  
451 equilibrium in the paired Pik NLRs. Here we demonstrated how allelic Pik NLR pairs  
452 have differentially coevolved and functionally specialized, leading to autoimmune  
453 phenotypes when mismatched. This suggests that in response to HMA integration  
454 and diversification in the sensor NLR Pik-1, its helper NLR Pik-2 has acquired  
455 polymorphisms to avoid loss of function and/or triggering autoimmunity.

456 To date, integrated domains have been primarily found in paired NLRs that are  
457 located in co-regulatory modules with a shared promoter region (Cesari et al., 2014a).  
458 Therefore, the spatial regulation of NLRs with unconventional domains in pairs might  
459 be a general mechanism to mitigate NLR misregulation as a consequence of domain  
460 integrations or their accelerated evolutionary rates compared with other NLR  
461 domains (Bialas et al., 2021).

462 We found mismatched allelic NLR pairs can lead to constitutive cell death. We further  
463 narrowed down this phenotype to a single Asp to Glu polymorphism, which is the  
464 same polymorphism that underpins an extended cell death response to AVR-Pik  
465 effectors. Introducing this Asp230Glu polymorphism in Pikp-2 led to an increase of  
466 cell death in response to AVR-Pik effectors as well as to autoimmune phenotypes. As  
467 these amino acids have very similar properties it is intriguing how a fairly minor  
468 difference can underpin such a major phenotype. The mechanistic basis of this  
469 autoactivation phenotype remains obscure, but it is possible that the larger amino acid  
470 side chain (Glu carries an extra methylene group in the side chain) is sufficient to  
471 perturb protein-protein interactions that support transition to the active state of the  
472 NLR pair. Analogous Asp to Glu changes have been previously shown to act as a gain-  
473 of-function mutation in response regulators and transcription factors (Sakai et al.,  
474 2001; To et al., 2007). In some cases, the Asp residue is a target of phosphorylation and  
475 the change to Glu partially acts as a phosphomimetic mutation that leads to an active  
476 form (Klose et al., 1993). However, to date, there is no evidence to suggest that  
477 phosphorylation of Asp230 is involved in Pikp-2 activation. The Asp to Glu change  
478 did not prevent sensor/helper association, although it affected association preference.  
479 Altogether, this illustrates that small changes in NLR receptors can have profound  
480 phenotypical effects on immune regulation and cell death responses.

481 We still lack detailed information about the activation mechanism of paired plant  
482 NLRs although a cooperation mechanism has been proposed for the Pik NLR pair  
483 (Zdrzalek et al., 2020). By taking advantage of constitutively active Pik sensor/helper  
484 combinations and mutants we can expand our knowledge of NLR signalling  
485 mechanisms. The use of constitutively active immune receptors as a research tool is

486 starting to be explored in the field of NLR biology. This approach has the advantage  
487 of simplifying the complex requirements of immune activation by removing the  
488 variability of the effector. It also renders full receptor activation, whilst relying solely  
489 on effector recognition can provide a mixture of active and inactive receptors.

490 Sensor and helper Pik NLRs form a pre-activation complex (Zdrzalek et al., 2020).  
491 Activation of immune responses may rearrange the composition of this complex,  
492 possibly affecting sensor/helper stoichiometry, as described for NAIP/NLRC4  
493 inflammasomes (Hu et al., 2015; Tenthorey et al., 2017; Zhang et al., 2015). This  
494 rearrangement is dependent on nucleotide binding and has been fine-tuned during  
495 the evolutionary process, as depicted in the competition assays in the Pik pair.

496 Autoactive mutations in Pikp-2 led us to re-evaluate the involvement of conserved p-  
497 loop and MHD motif of sensor and helper Pik NLRs in signalling activation. In  
498 contrast to the previously described cooperation mechanism of Pik regulation (Bialas  
499 et al., 2018; Zdrzalek et al., 2020), the p-loop of sensor NLR Pik-1 is important but not  
500 necessary for NLR activation. This also deviates from the negative regulation  
501 mechanism described for other NLR pairs such as Pia or Arabidopsis RRS1/RPS4  
502 (Cesari et al., 2014b; Cesari et al., 2013; Le Roux et al., 2015; Sarris et al., 2015) and  
503 suggests the Pik pair may trigger cell death via a different mechanism. Future  
504 experiments using autoactive combinations should help unravel the requirements of  
505 Pik NLR immune signalling and will reveal the nature of the changes undergone by  
506 NLRs during activation.

507 In summary, this work provides an evolutionary framework for how differential  
508 selective pressures, such as recognition of pathogen strains via effector binding,  
509 impact NLRs pairs. It uncovers the potential of paired NLRs to give rise to  
510 autoimmune phenotypes during evolution and links pathogen perception and  
511 autoimmunity.

## 512 **Materials and Methods**

### 513 **Phylogenetics analyses.**

514 Codon-based alignment was generated using MUSCLE 3.8.425 (Edgar, 2004). The  
515 alignment positions with more than 40% data missing were removed using  
516 QKphylogeny (<https://github.com/matthewmoscou/QKphylogeny>). The maximum  
517 likelihood tree was calculated from a 3,066-nt-long alignment using 1000 bootstrap  
518 method (Felsenstein, 1985) and GTRGAMMA substitution model (Tavaré, 1986) as  
519 implemented in RAxML v8.2.11 (Stamatakis, 2014). Best-scoring tree was manually  
520 rooted using the Pik-2 sequence from *Leersia perreri* and visualized using the iTOL tool  
521 v5.5.1 (Letunic and Bork, 2019). The interactive tree is publicly available at:  
522 <https://itol.embl.de/tree/8229133147185181615486010>

523 Joint reconstruction of ancestral sequences (Yang et al., 1995), based on the algorithm  
524 of Pupko et al. (Pupko et al., 2000), was performed using the codeml program as part  
525 of the PAML 4.9j package (Yang, 1997). The ancestral sequence reconstruction was  
526 carried out based on best-scoring ML tree and a 3,261-nt-long codon alignment of the  
527 full length Pik-2 sequences.

528 The accession numbers of the sequences used in the phylogenetic analyses are  
529 LPERR11G19580.2, ONIVA11G22700, ORUFI11G24740, XM\_015762499.2,  
530 OGLUM11G22330, ORGLA11G0185700, MW568036, MW568041, MW568042,  
531 MW568043, MW568044, MW568045, KN541092.1, OPUNC11G19560,  
532 OBART11G23160.1, GU811862, HQ606329, HM048900\_1, HQ662329\_1, GU811867,  
533 AB462325, GU811861, GU811864, GU811865, GU811866, HQ662330, HM035360,  
534 KU365338.1, HQ660231, GU811868, GU811869, GU811870, GU811871, GU811872.

### 535 **Gene cloning.**

536 For protein expression in planta, we used full length Pikp-1 and Pikm-1 into the  
537 plasmid pICH47742 with a C-terminal 6×His/3×FLAG tag as previously described (De  
538 la Concepcion et al., 2018). Wild-type Pikp-2 and Pikm-2 in pICH47751 with C-  
539 terminal 6×HA were also described in (De la Concepcion et al., 2018) and Pik-2  
540 mutated versions were generated by site-directed mutagenesis (see below) using

541 appropriate Pik-2 template in pCR8/GW/TOPO (Invitrogen) with Golden Gate  
542 compatible overhangs. The constructs were later assembled in pICH47751 under  
543 control of *Agrobacterium tumefaciens* mannopine synthase (Mas) promoter and  
544 terminator and a C-terminal 6xHA using golden gate cloning (Engler et al., 2014).  
545 AVR-Pik effector alleles used in this study were previously described in (De la  
546 Concepcion et al., 2018).

547 All DNA constructs were verified by sequencing.

#### 548 **Site-directed mutagenesis.**

549 Point mutations were introduced in Pik-2 by PCR amplification with Phusion™  
550 polymerase (Thermo Fisher Scientific) using 5'-phosphorylated primers carrying the  
551 desired mutations. The amplification used primers running in opposite directions  
552 from the mutation site in the template Pik-2 in pCR8/GW/TOPO vector (Invitrogen).  
553 DNA templates were then eliminated by incubating the reaction with DpnI (New  
554 England Biolabs) for 1h at 37 °C. After PCR purification of the amplified products, the  
555 DNA sequence was re-ligated using T4 DNA ligase (New England Biolabs) according  
556 to the manufacturer's protocol in 20 µl reactions incubated overnight at room  
557 temperature. Competent *E. coli* DH5α cells were subsequently transformed with 5 µl  
558 of the reaction. The resulting constructs were sequenced to ensure that a correct  
559 mutation was inserted into the sequence.

#### 560 **in planta co-immunoprecipitation (Co-IP).**

561 Transient gene-expression in planta for Co-IP was performed by delivering T-DNA  
562 constructs with *A. tumefaciens* GV3101 (C58 (rifR) Ti pMP90 (pTiC58DT-DNA) (gentR)  
563 Nopaline (pSoup-tetR)) strain into 4-week-old *N. benthamiana* plants grown at 22–25°C  
564 with high light intensity. *A. tumefaciens* strains carrying the given wild-type or  
565 mutated Pik-1 or Pik-2 were infiltrated at OD<sub>600</sub> 0.2 each (unless otherwise stated), in  
566 agroinfiltration medium (10 mM MgCl<sub>2</sub>, 10 mM 2-(N-morpholine)-ethanesulfonic acid  
567 (MES), pH 5.6), supplemented with 150 µM acetosyringone.

568 For detection of complexes in planta, leaf tissue was collected 2–3 days post infiltration  
569 (dpi), frozen, and ground to fine powder in liquid nitrogen using a pestle and mortar.

570 Leaf powder was mixed with 2 times weight/volume ice-cold extraction buffer (10%  
571 glycerol, 25 mM Tris pH 7.5, 1 mM EDTA, 150 mM NaCl, 2% w/v PVPP, 10 mM DTT,  
572 1× protease inhibitor cocktail (Sigma), 0.1% Tween 20 (Sigma)), centrifuged at 4,200g  
573 at 4°C for 20–30 min, and the supernatant was passed through a 0.45 µm Minisart®  
574 syringe filter. The presence of each protein in the input was determined by SDS-  
575 PAGE/western blot. Wild-type and mutated Pik-1 and Pik-2 proteins were detected  
576 probing the membrane with anti-FLAG M2 antibody (Sigma) and anti-HA high  
577 affinity antibody 3F10 (Roche), respectively. For detection of Pikm-2 in the  
578 competition experiments in planta, we used anti-V5 antibody HRP-conjugated  
579 (Invitrogen).

580 For immunoprecipitation, 1.5 ml of filtered plant extract was incubated with 30 µl of  
581 M2 anti-FLAG resin (Sigma) in a rotatory mixer at 4°C. After three hours, the resin  
582 was pelleted (800g, 1 min) and the supernatant removed. The pellet was washed and  
583 resuspended in 1 ml of IP buffer (10% glycerol, 25 mM Tris pH 7.5, 1 mM EDTA, 150  
584 mM NaCl, 0.1% Tween 20 (Sigma)) and pelleted again by centrifugation as before.  
585 Washing steps were repeated 5 times. Finally, 30 µl of LDS Runblue® sample buffer  
586 was added to the agarose and incubated for 10 min at 70°C. The resin was pelleted  
587 again, and the supernatant loaded on SDS-PAGE gels prior to western blotting.  
588 Membranes were probed with anti-FLAG M2 antibody (Sigma) and anti-HA high  
589 affinity antibody 3F10 (Roche) monoclonal antibodies. For competition experiments,  
590 the membrane was additionally probed with anti-V5 antibody HRP-conjugated  
591 (Invitrogen) to detect Pikm-2.

#### 592 *N. benthamiana* cell death assays.

593 *A. tumefaciens* GV3101 (C58 (rifR) Ti pMP90 (pTiC58DT-DNA) (gentR) Nopaline  
594 (pSoup-tetR)) carrying wild-type or mutated Pik-1, Pik-2 were resuspended in  
595 agroinfiltration media (10 mM MgCl<sub>2</sub>, 10 mM 2-(N-morpholine)-ethanesulfonic acid  
596 (MES), pH 5.6) supplemented with 150 µM acetosyringone. Given combinations of  
597 Pik-1 and Pik-2 constructs were mixed at OD<sub>600</sub> 0.4 for each construct. *A. tumefaciens*  
598 GV3101 carrying AVR-Pik effectors or mCherry were added to each experiment at  
599 OD<sub>600</sub> 0.6. Each infiltration had additional *A. tumefaciens* GV3101 (C58 (rifR) Ti pMP90

600 (pTiC58DT-DNA) (gentR) Nopaline (pSoup-tetR)) carrying P19 at OD<sub>600</sub> 0.1. Leaves  
601 of 4-weeks-old *N. benthamiana* were infiltrated using a needleless syringe. Leaves were  
602 collected at 5 dpi to measure UV autofluorescence as proxy for cell death as reported  
603 previously (De la Concepcion et al., 2019; De la Concepcion et al., 2018; Maqbool et al.,  
604 2015).

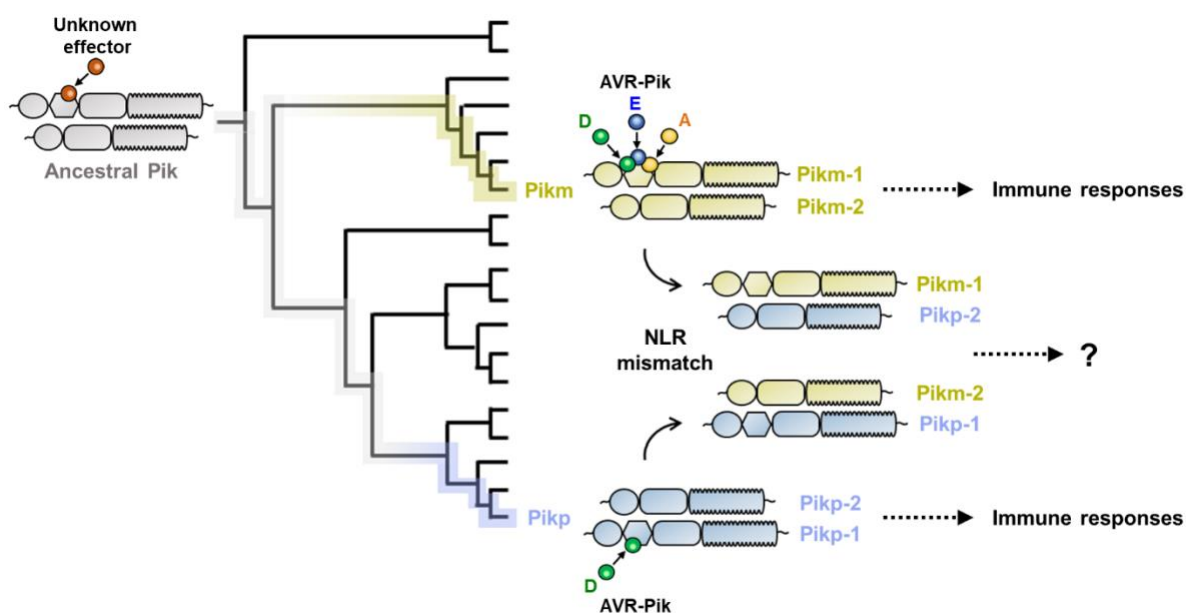
#### 605 **Cell death scoring: UV autofluorescence.**

606 Detached leaves were imaged at 5 dpi from the abaxial side of the leaves for UV  
607 fluorescence images. Photos were taken using a Nikon D4 camera with a 60 mm macro  
608 lens, ISO set 1600 and exposure ~10 secs at F14. The filter is a Kodak Wratten No.8 and  
609 white balance is set to 6250 degrees Kelvin. Blak-Ray® longwave (365nm) B-100AP  
610 spotlight lamps are moved around the subject during the exposure to give an even  
611 illumination. Images shown are representative of three independent experiments,  
612 with internal repeats. The cell death index used for scoring is as presented previously  
613 (Maqbool et al., 2015). Dotplots were generated using R v3.4.3 ([https://www.r-](https://www.r-project.org/)  
614 [project.org/](https://www.r-project.org/)) and the graphic package ggplot2 (Wickham, 2016). The size of the centre  
615 dot at each cell death value is directly proportional to the number of replicates in the  
616 sample with that score. All individual data points are represented as dots.



## 617 **Acknowledgments**

618 We thank present and former members of the Banfield and Kamoun laboratories for  
619 discussions that have shaped this manuscript, and colleagues at Iwate Biotechnology  
620 Research Center for stimulating discussions on NLR biology. We specially thank Dr.  
621 Cristina Barragan and Dr. Adam Bentham for critical reading of the manuscript. We  
622 also thank Andrew Davies and Phil Robinson from JIC Scientific Photography for the  
623 UV pictures of the cell death assays. This work was supported by the Biotechnology  
624 and Biological Sciences Research Council (BBSRC, UK, grant BB/012574,  
625 BBS/E/J/000PR9795), the BBSRC Doctoral Training Partnership at Norwich Research  
626 Park (grant: BB/M011216/1, project reference 1771322), the European Research  
627 Council (proposal 743165), the John Innes Foundation, the Gatsby Charitable  
628 Foundation, the European Commission through the Erasmus+ programme, and JSPS  
629 Grant 20H05681.



630

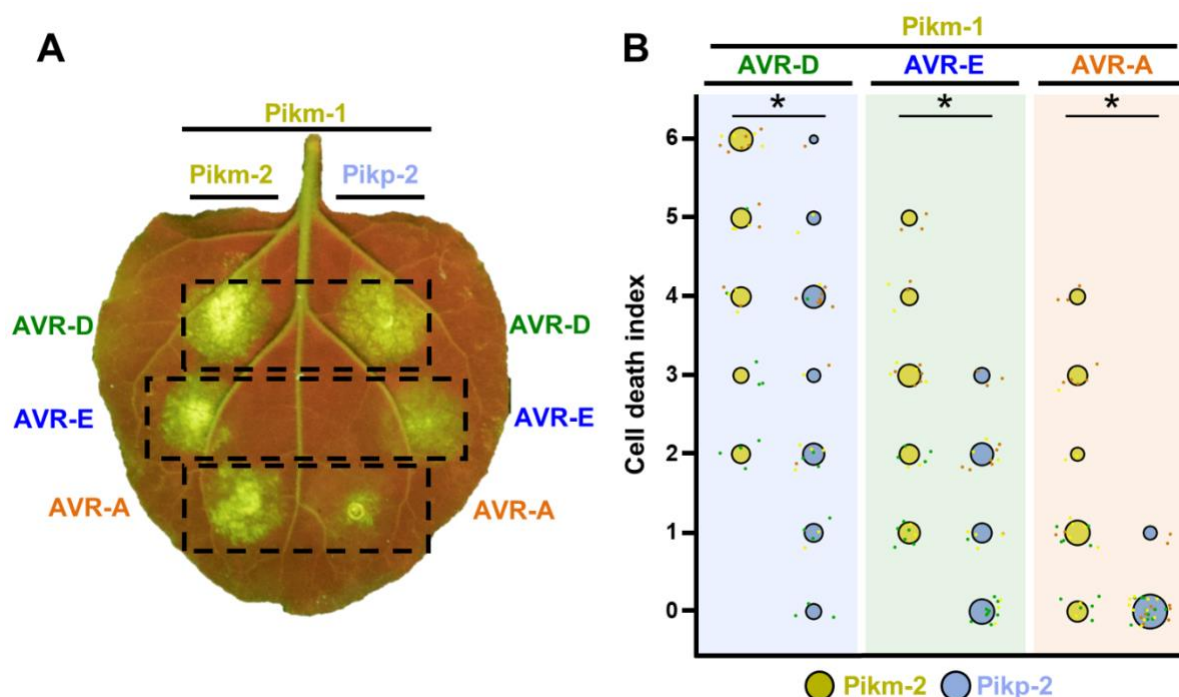
631 **Figure S1. Schematic representation of the hypothesis tested in this study.** Sensor

632 NLR alleles *Pikp-1* and *Pikm-1* convergently evolved to bind *M. oryzae* AVR-Pik

633 effectors, triggering immune responses together with their corresponding NLR pair.

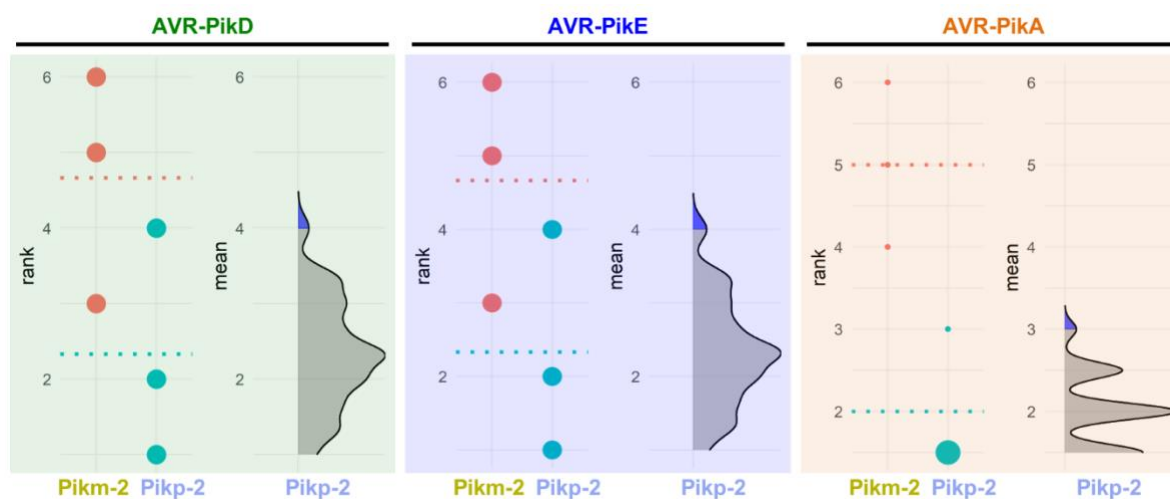
634 We tested sensor/helper specificity in *Pikp* and *Pikm* pairs by mismatching allelic

635 receptor and measuring immune response outcomes.



636

637 **Figure 1. Pikm-1 elicits a stronger response to the AVR-Pik effectors when it is**  
638 **paired with Pikm-2 than with Pikp-2. (A)** Representative *N. benthamiana* leaf  
639 depicting Pik-mediated cell death as autofluorescence under UV light. Pikm-1 was co-  
640 expressed with either Pikm-2 or Pikp-2 and the AVR-Pik effector alleles recognized  
641 by Pikm. Side-by-side infiltrations are highlighted with dashed boxes. **(B)** Scoring of  
642 cell death triggered by Pikp-2 or Pikm-2 with each AVR-PikD (AVR-D), AVR-PikE  
643 (AVR-E) and AVR-PikA (AVR-A) is represented as dot plots. The total number of  
644 repeats was 30. For each sample, all the data points are represented as dots with a  
645 distinct colour for each of the three biological replicates; these dots are jittered around  
646 the cell death score for visualisation purposes. The size of the central dot at each cell  
647 death value is proportional to the number of replicates of the sample with that score.  
648 Significant differences between relevant conditions are marked with an asterisk and  
649 the details of the statistical analysis are summarised in **Figure S2**.



650

651 **Figure S2. Estimation graphics for comparison of cell death mediated by Pikm-1**

652 **when co-expressed with Pikm-2 or Pikip-2.** Statistical analysis by estimation methods

653 of the cell death assay for Pikm-1 co-expressed with Pikm-2 or Pikip-2 and AVR-PikD,

654 AVR-PikE or AVR-PikA. For each effector, the panel on the left represents the ranked

655 data (dots) for each NLR, and their corresponding mean (dotted line). The size of the

656 dots is proportional to the number of observations with that specific value. The panel

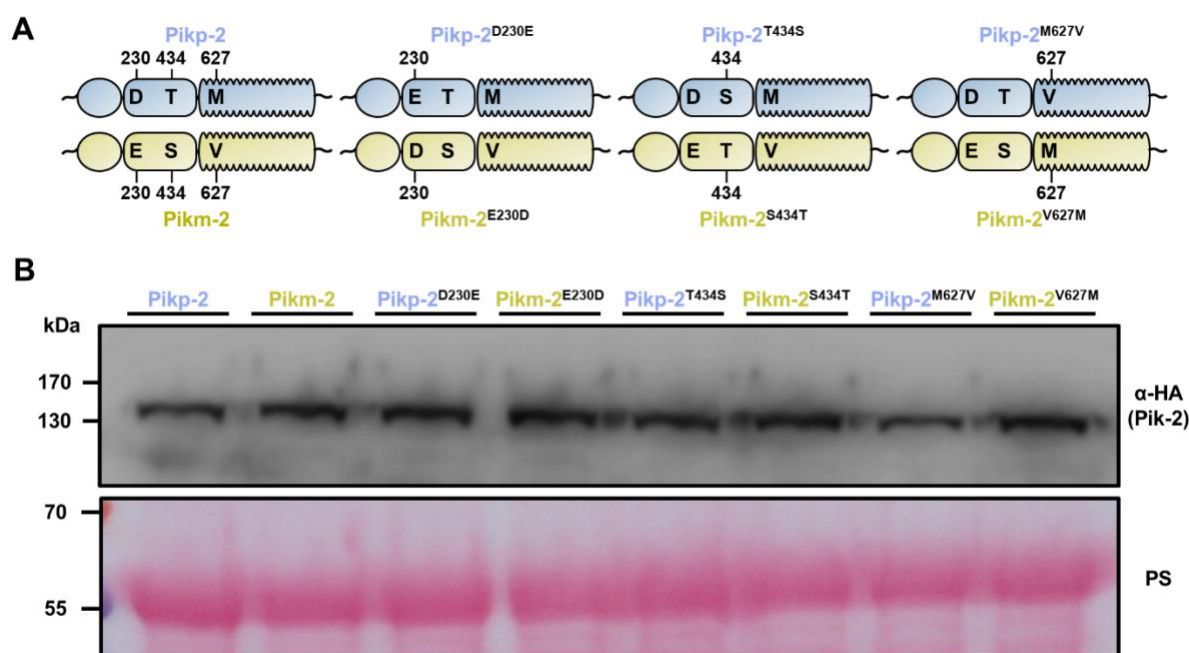
657 on the right shows the distribution of 1000 bootstrap sample rank means for Pikm-1

658 paired with Pikip-2. The blue areas represent the 0.025 and 0.975 percentiles of the

659 distribution. Pikm-1 mediated responses with Pikm-2 or Pikip-2 are considered

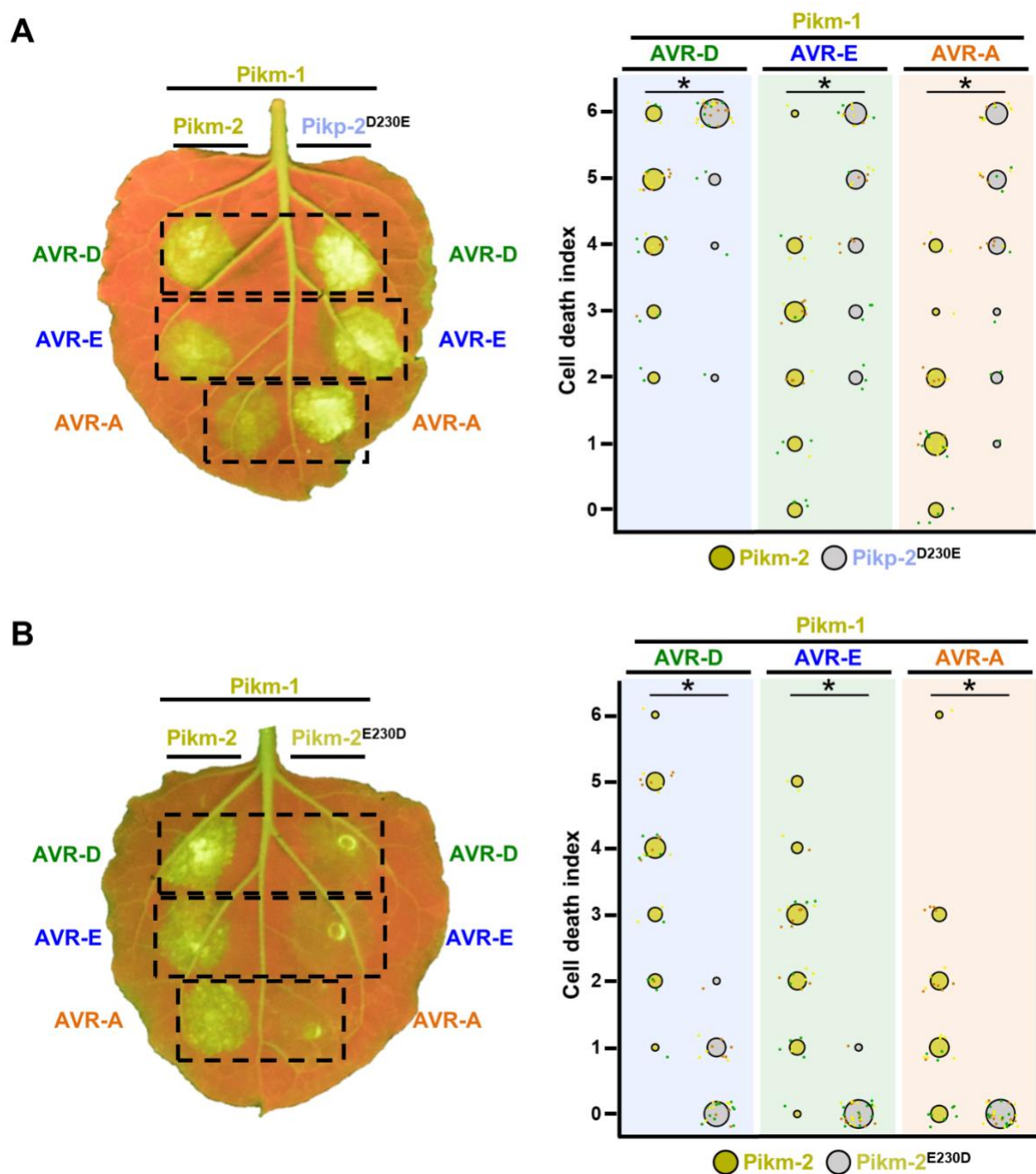
660 significantly different if the Pikm-2 rank mean (dotted line, left panel) falls beyond the

661 blue regions of the Pikip-2 mean distribution.



662

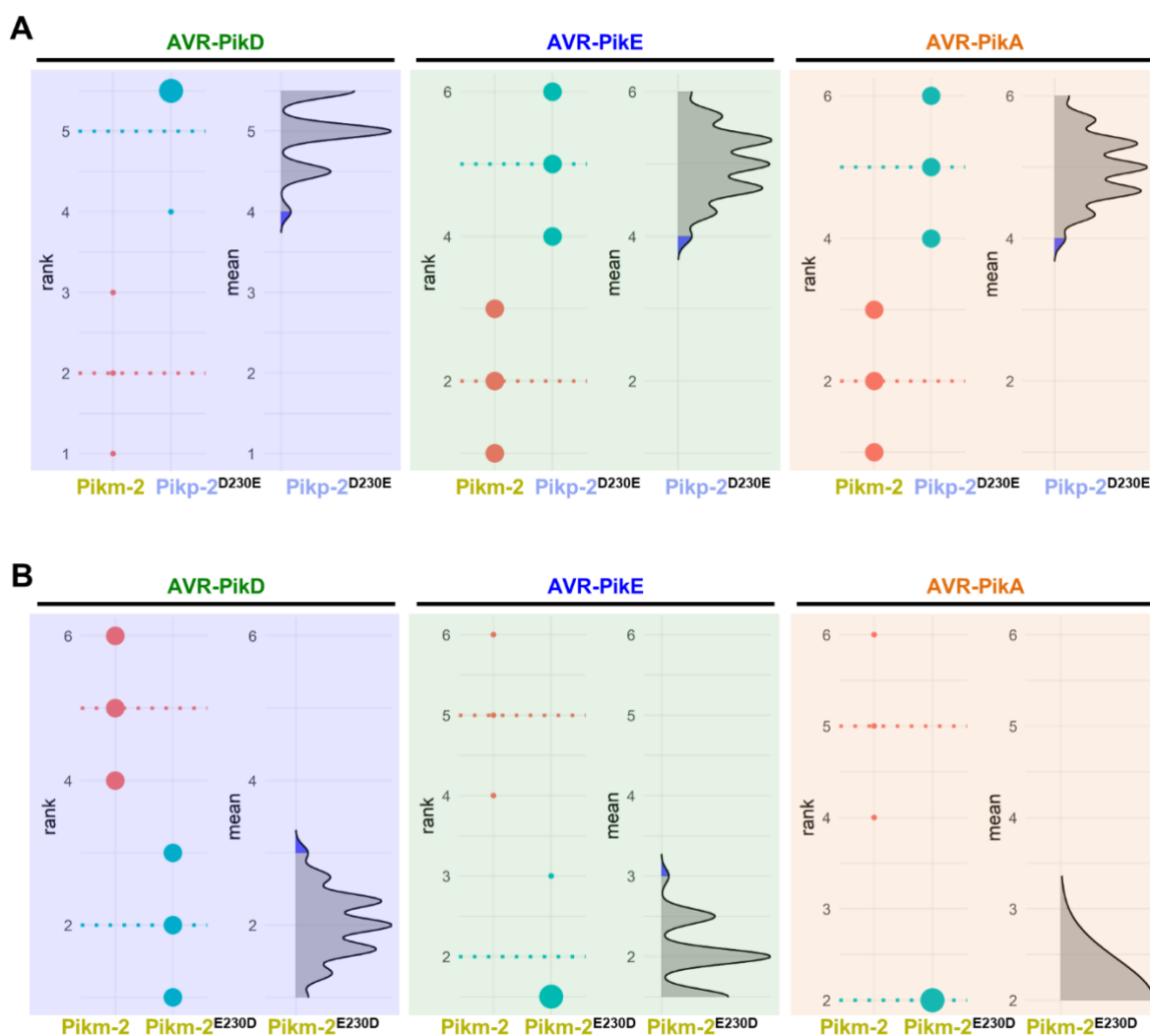
663 **Figure S3. The *Pik-2* alleles and mutants have similar levels of protein accumulation**  
664 **in planta.** (A) Schematic representations of polymorphism distribution in the *Pik-2*  
665 allelic NLRs and their mutants. Polymorphic sites are numbered. (B) Western blots  
666 showing accumulation of wild-type *Pikp-2* and *Pikm-2* and point mutants. C-  
667 terminally 6xHA tagged *Pik-2* proteins were transiently expressed *N. benthamiana*.  
668 Total protein extracts were probed with  $\alpha$ -HA antisera. Total protein loading is shown  
669 by Ponceau staining (PS).



670

671 **Figure 2. A single Pik-2 polymorphism modulates the cell death response to the**  
 672 **AVR-Pik effectors.** Representative leaves depicting cell death mediated by Pik-2  
 673 mutants as autofluorescence under UV light. Pikm-1 was co-expressed with either **(A)**  
 674 Pikp-2 Asp230Glu or **(B)** Pikm-2 Glu230Asp and AVR-PikD (AVR-D), AVR-PikE  
 675 (AVR-E) or AVR-PikA (AVR-A). Side-by-side infiltrations with Pikm NLR pair are  
 676 highlighted with dashed boxes for comparison. Cell death scoring is represented as  
 677 dot plots. The number of repeats was 30. For each sample, all the data points are  
 678 represented as dots with a distinct colour for each of the three biological replicates;

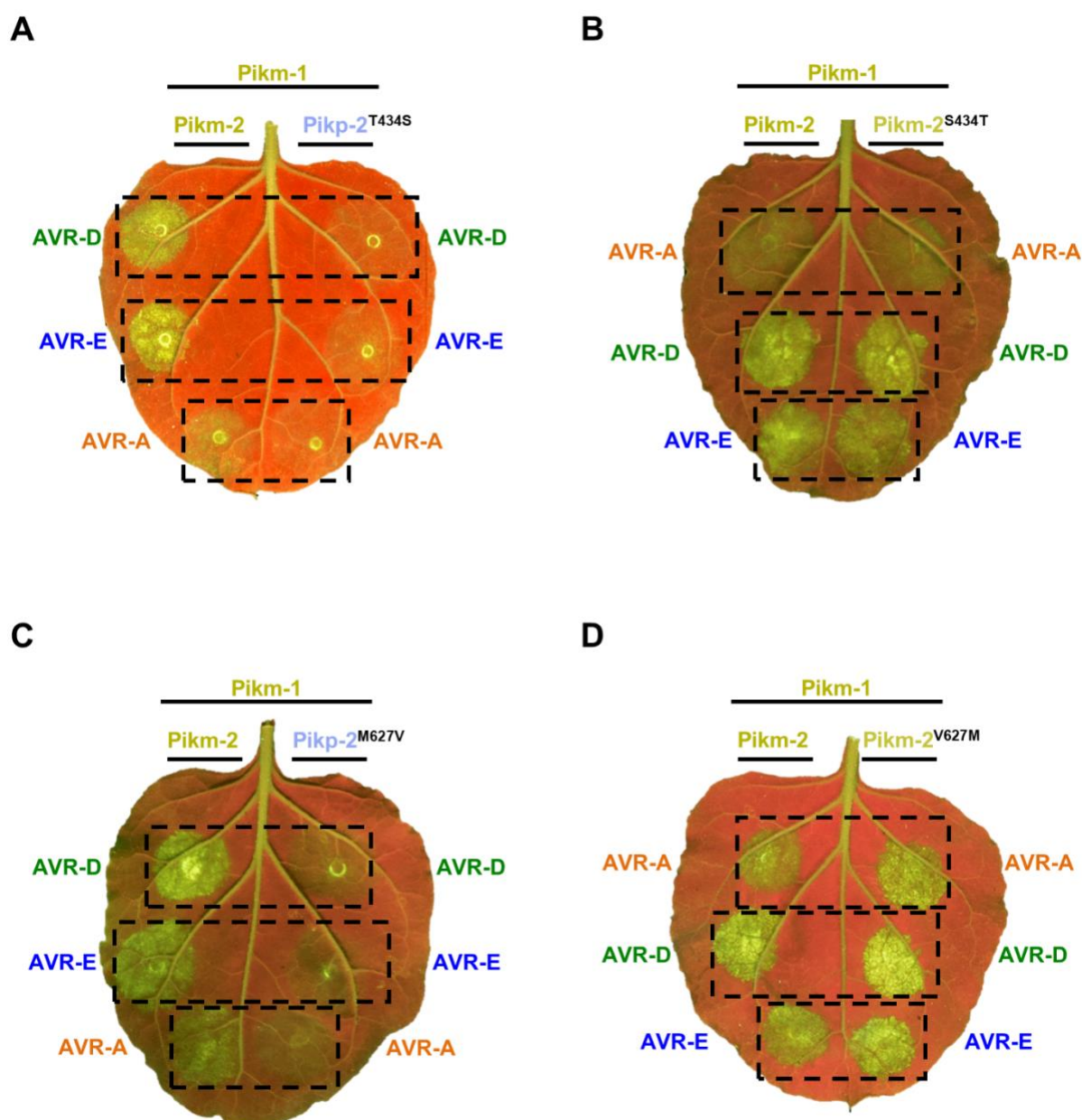
679 these dots are jittered about the cell death score for visualisation purposes. The size of  
680 the central dot at each cell death value is proportional to the number of replicates of  
681 the sample with that score. Significant differences between relevant conditions are  
682 marked with an asterisk and the details of the statistical analysis are summarised in  
683 **Figure S4.**



684

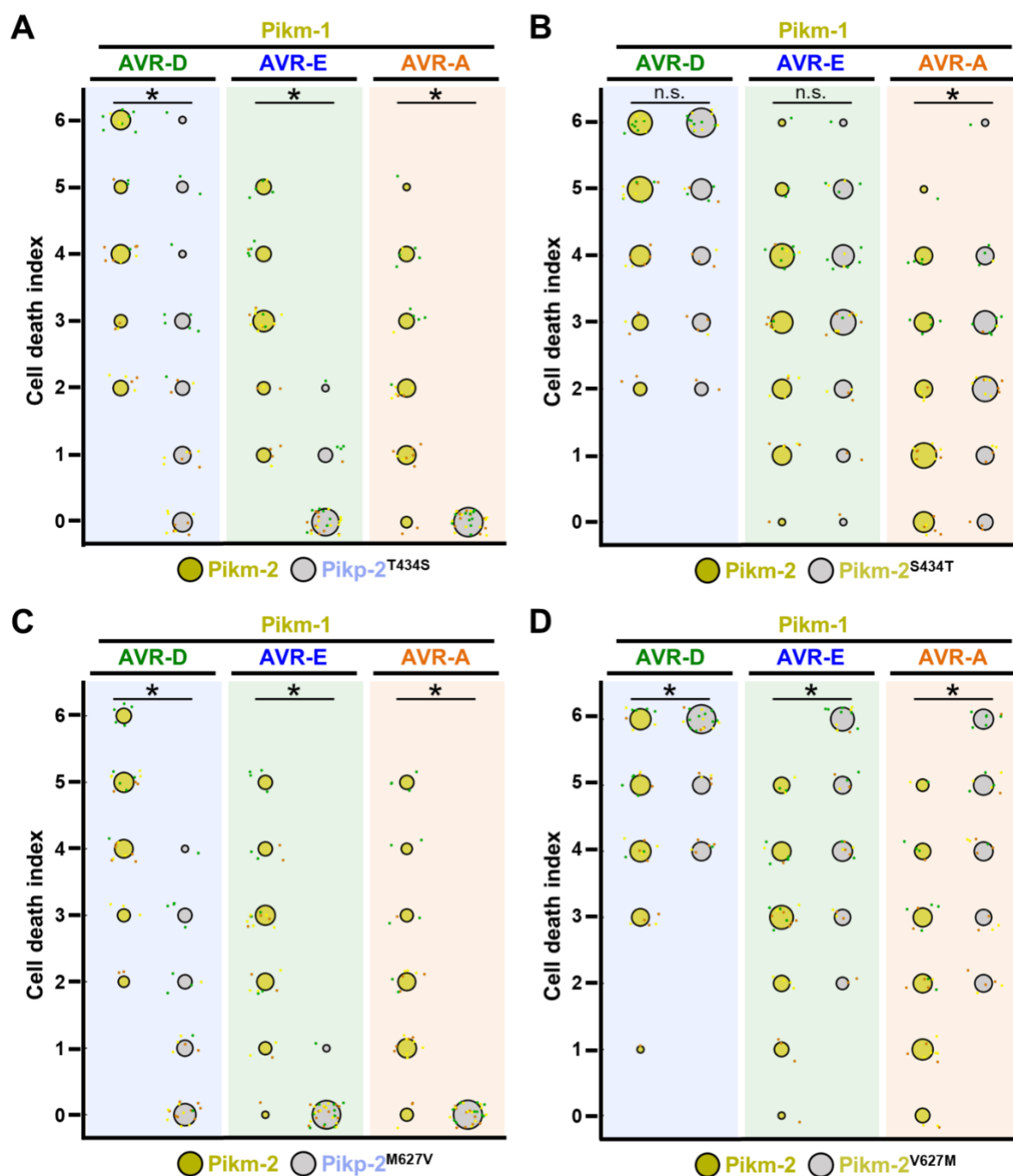
685 **Figure S4. Estimation graphics for comparison of cell death mediated by Pikm-1**  
 686 **when co-expressed with the Pikm-2 or Pik-2 mutants in the polymorphic position**  
 687 **230. Statistical analysis by estimation methods of the cell death assay for Pikm-1 co-**  
 688 **expressed with (A) Pikp-2 Asp230Glu or (B) Pikm-2 Glu230Asp and AVR-PikD, AVR-**  
 689 **PikE or AVR-PikA, compared with wild-type Pikm-2. For each effector, the panel on**  
 690 **the left represents the ranked data (dots) for each NLR, and their corresponding mean**  
 691 **(dotted line). The size of the dots is proportional to the number of observations with**  
 692 **that specific value. The panel on the right shows the distribution of 1000 bootstrap**  
 693 **sample rank means for Pikm-1 paired with a Pik-2 mutant. The blue areas represent**  
 694 **the 0.025 and 0.975 percentiles of the distribution. Pikm-1 mediated responses with**  
 695 **Pikm-2 or Pik-2 mutant are considered significantly different if the Pikm-2 rank mean**  
 696 **(dotted line, left panel) falls beyond the blue regions in the mean distribution of the**  
 697 **Pik-2 mutants.**





698

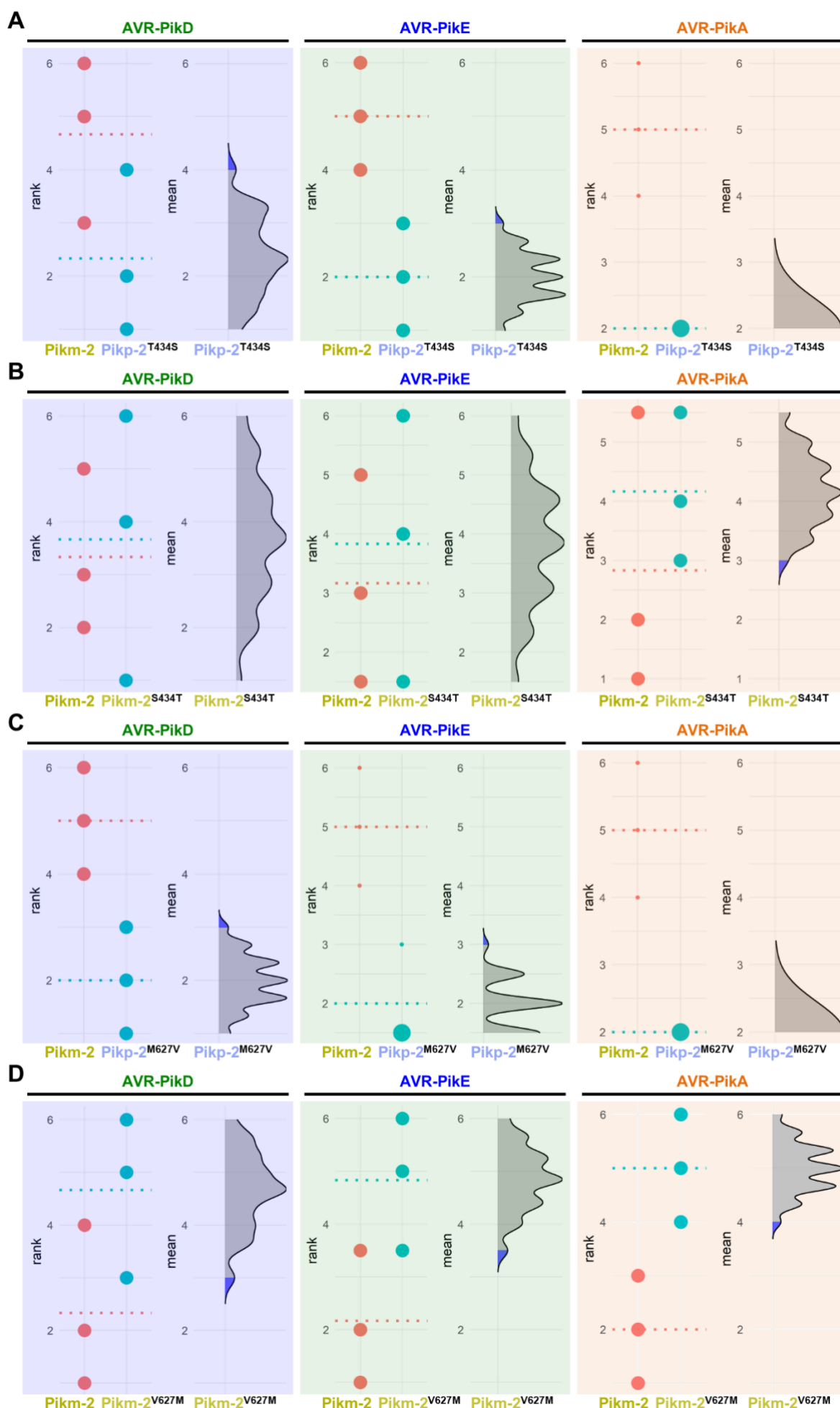
699 **Figure S5. Representative images of cell death mediated by the Pik-2 mutants in**  
700 **response to the AVR-Pik effectors.** Representative leaves depicting cell death  
701 mediated by Pik-2 mutants as autofluorescence under UV light. Pikm-1 was co-  
702 expressed with either (A) Pikp-2 Asp230Glu, (B) Pikm-2 Glu230Asp, (C) Pikp-2  
703 Asp230Glu and (D) Pikm-2 Glu230Asp and AVR-PikD (AVR-D), AVR-PikE (AVR-E)  
704 or AVR-PikA (AVR-A). Side-by-side infiltrations with the Pikm NLR pair are  
705 highlighted with dashed boxes for comparison.



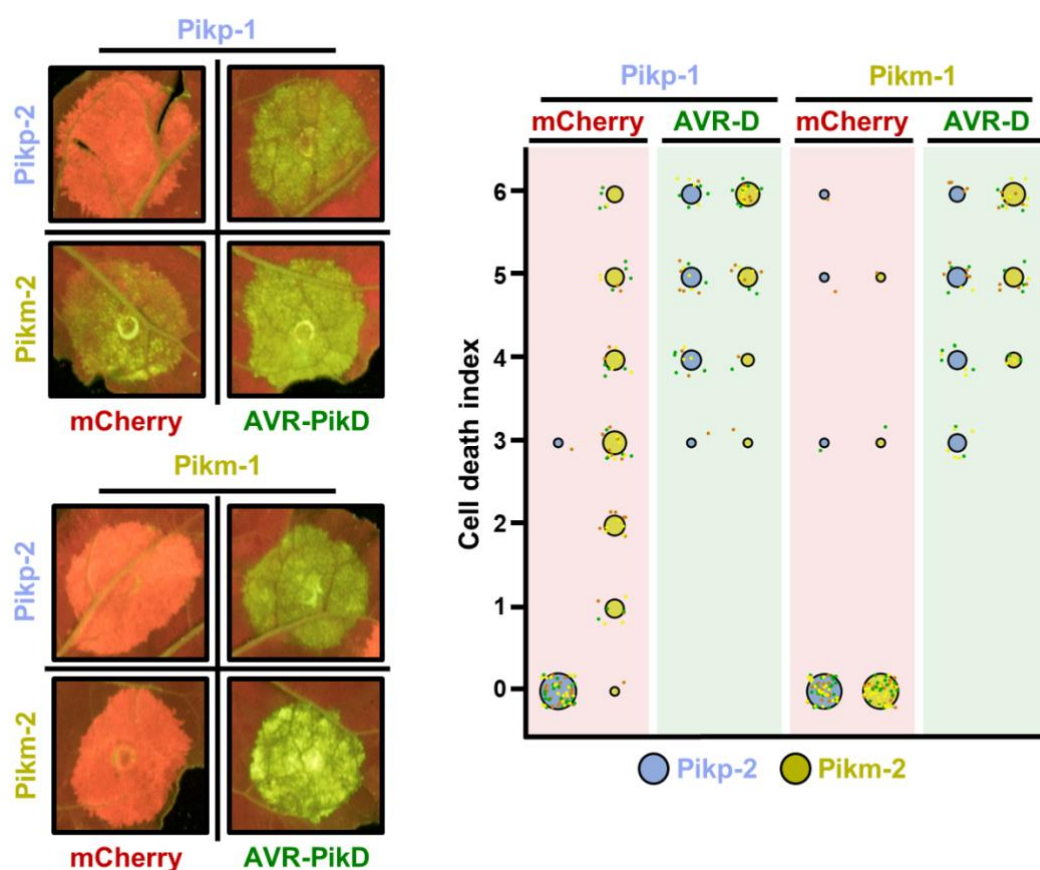
706

707 **Figure S6. Quantification of cell death mediated by the Pik-2 mutants in response**  
 708 **to AVR-Pik effectors.** Cell death scoring is represented as dot plots comparing cell  
 709 death triggered by the Pik-2 mutants **(A)** Pikm-2 Thr434Ser, **(B)** Pikm-2 Ser434Thr, **(C)**  
 710 Pikp-2 Met627Val and **(D)** Pikm-2 Val627Met. The mutants were co-expressed with  
 711 Pikm-1 and AVR-PikD, AVR-PikE or AVR-PikA. Pikm NLR pair was co-infiltrated for  
 712 side-by-side comparison. The number of repeats was 30. For each sample, all the data  
 713 points are represented as dots with a distinct colour for each of the three biological  
 714 replicates; these dots are jittered about the cell death score for visualisation purposes.

715 The size of the central dot at each cell death value is proportional to the number of  
716 replicates of the sample with that score. Significant differences between relevant  
717 conditions are marked with an asterisk and the details of the statistical analysis are  
718 summarised in **Figure S7**.

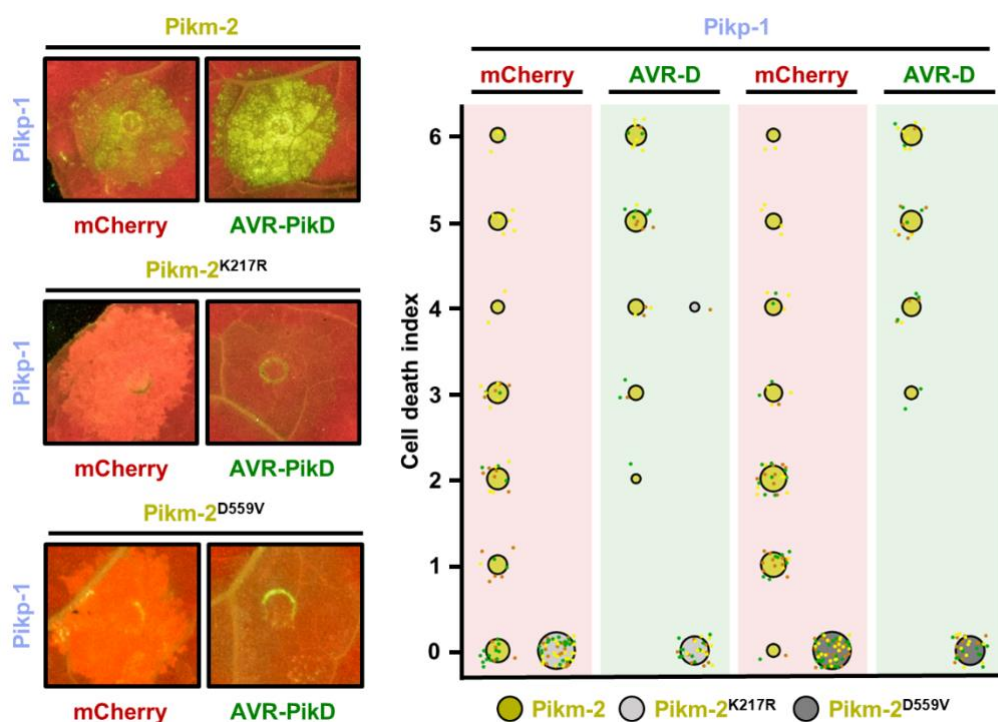


720 **Figure S7. Estimation graphics for comparison of cell death mediated by Pikm-1**  
721 **when co-expressed with Pikm-2 or Pik-2 mutants in polymorphic position 434 and**  
722 **627.** Statistical analysis by estimation methods of the cell death assay for Pikm-1 co-  
723 expressed with **(A)** Pikp-2 Thr434Ser, **(B)** Pikm-2 Ser434Thr, **(C)** Pikp-2 Met627Val or  
724 **(D)** Pikm-2 Val627Met and AVR-PikD, AVR-PikE or AVR-PikA, compared with wild-  
725 type Pikm-2. For each effector, the panel on the left represents the ranked data (dots)  
726 for each NLR, and their corresponding mean (dotted line). The size of the dots is  
727 proportional to the number of observations with that specific value. The panel on the  
728 right shows the distribution of 1000 bootstrap sample rank means for Pikm-1 paired  
729 with a Pik-2 mutant. The blue areas represent the 0.025 and 0.975 percentiles of the  
730 distribution. Pikm-1 mediated responses with Pikm-2 or Pik-2 mutant are considered  
731 significantly different if the Pikm-2 rank mean (dotted line, left panel) falls beyond the  
732 blue regions in the mean distribution of the Pik-2 mutants.



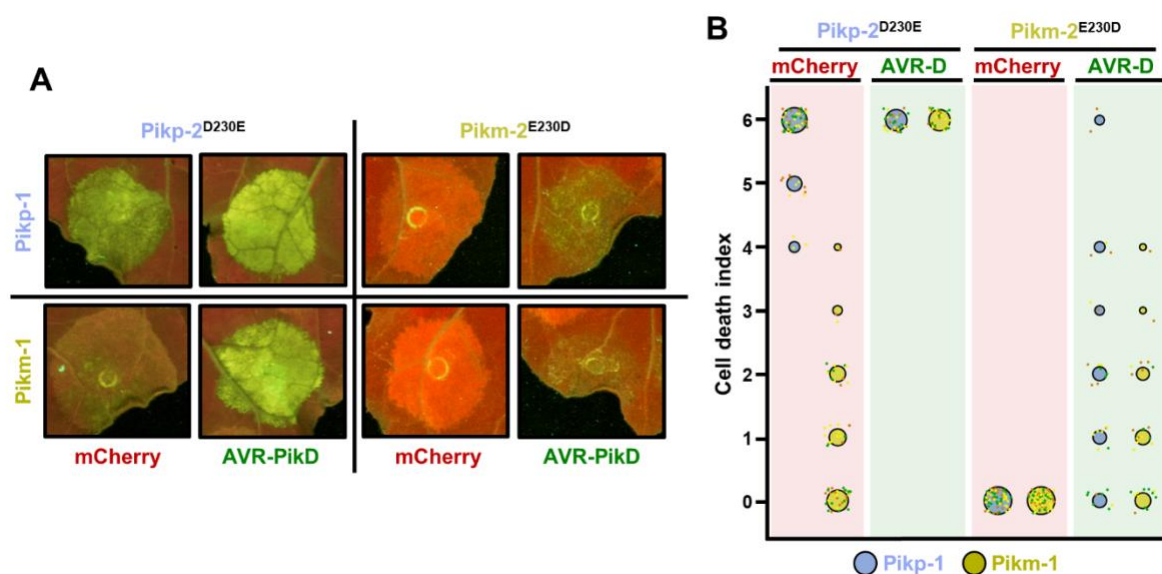
733

734 **Figure 3. Pikm-2 triggers constitutive cell death in the presence of Pikp-1.**  
 735 Representative leaf spot images and scoring of Pik mediated cell death as  
 736 autofluorescence under UV-light in the presence or absence of AVR-PikD. Cell death  
 737 assay scoring represented as dot plots comparing cell death triggered by Pikp-2 and  
 738 Pikm-2 when co-expressed with Pikp-1 or Pikm-1. The number of repeats was 60 and  
 739 30 for the spots co-infiltrated with mCherry and AVR-PikD, respectively. For each  
 740 sample, all the data points are represented as dots with a distinct colour for each of  
 741 the three biological replicates; these dots are jittered about the cell death score for  
 742 visualisation purposes. The size of the central dot at each cell death value is  
 743 proportional to the number of replicates of the sample with that score.



744

745 **Figure 4. Constitutive cell death in mismatched Pik pairs is dependent on P-loop**  
746 **and MHD motifs.** Representative leaf spot images and scoring of Pikm-2 mediated  
747 cell death as autofluorescence under UV-light. Cell death scoring is represented as dot  
748 plots comparing cell death triggered by Pikm-2 mutant in P-loop (Lys217Arg) and  
749 MHD (Asp559Val) motifs and wild-type Pikm-2. Mutants and wild-type proteins  
750 were co-expressed with Pikp-1 and mCherry (red panel) or AVR-PikD (green panel).  
751 The number of repeats was 60 and 30 for the spots co-infiltrated with mCherry and  
752 AVR-PikD, respectively. For each sample, all the data points are represented as dots  
753 with a distinct colour for each of the three biological replicates; these dots are jittered  
754 about the cell death score for visualisation purposes. The size of the central dot at each  
755 cell death value is proportional to the number of replicates of the sample with that  
756 score.



757

758 **Figure 5. Polymorphism at position 230 in the NB-ARC domain is a Pik-2**

759 **determinant for constitutive cell death. (A)** Representative leaf spot images and

760 scoring of cell death mediated by Pik-2 as autofluorescence under UV-light. **(B)** Cell

761 death scoring is represented as dot plots comparing cell death triggered by Pik-2

762 mutants at polymorphic positions 230. Pik-2 mutants were co-expressed with Pikp-1

763 (blue dots) or Pikm-1 (yellow dots) together with mCherry (red panel) or AVR-PikD

764 (green panel). The number of repeats was 60 and 30 for the spots co-infiltrated with

765 mCherry and AVR-PikD, respectively. For each sample, all the data points are

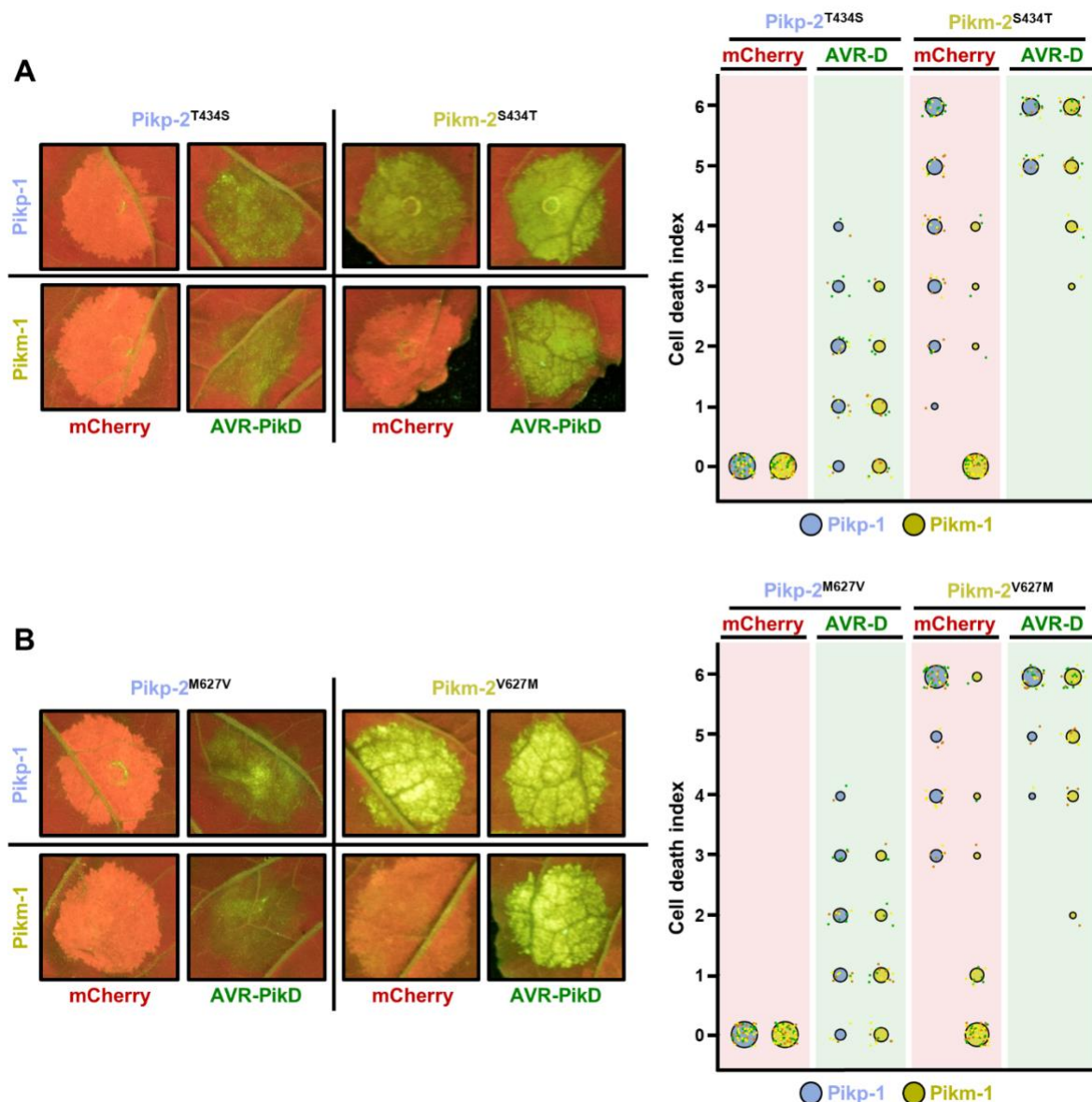
766 represented as dots with a distinct colour for each of the three biological replicates;

767 these dots are jittered about the cell death score for visualisation purposes. The size of

768 the central dot at each cell death value is proportional to the number of replicates of

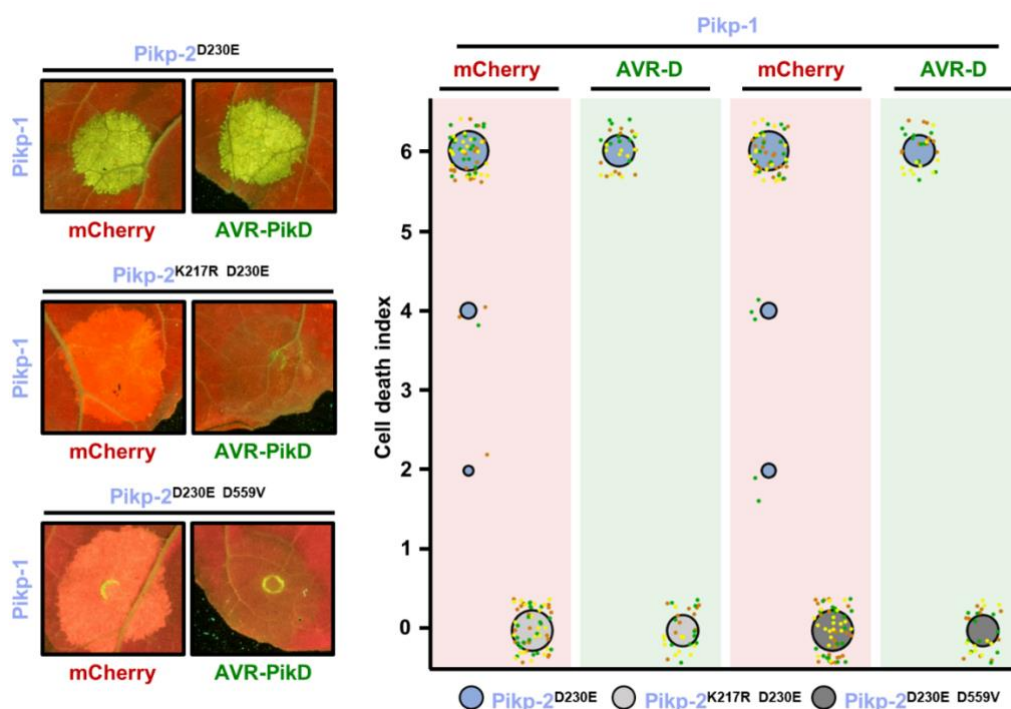
769 the sample with that score.





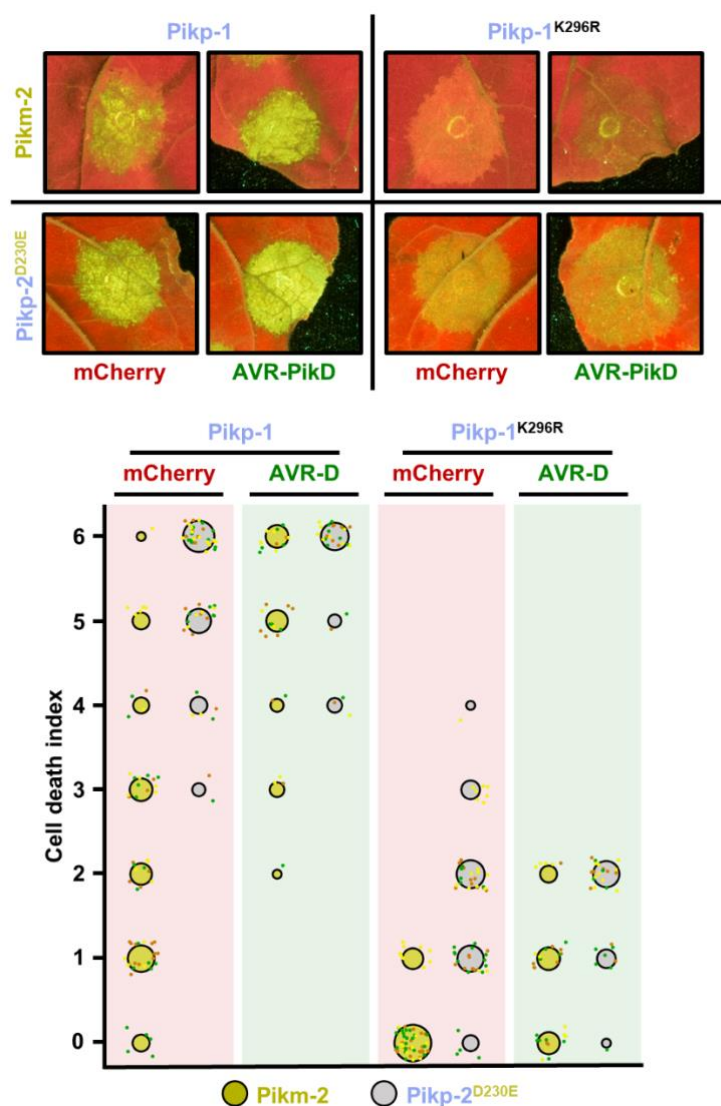
770

771 **Figure S8. The Pik-2 polymorphisms at position 434 and 627 do not alter constitutive**  
772 **cell death.** Representative leaf spot images and scoring of cell death mediated by Pik-  
773 2 as autofluorescence under UV-light. Cell death scoring is represented as dot plots  
774 comparing cell death triggered by Pik-2 mutants at polymorphic positions (A) 434 and  
775 (B) 627. Pik-2 mutants were co-expressed with Pikp-1 (blue dots) or Pikm-1 (yellow  
776 dots) together with mCherry (red panel) or AVR-PikD (green panel). The number of  
777 repeats was 60 and 30 for the spots co-infiltrated with mCherry and AVR-PikD,  
778 respectively. For each sample, all the data points are represented as dots with a distinct  
779 colour for each of the three biological replicates; these dots are jittered about the cell  
780 death score for visualisation purposes. The size of the central dot at each cell death  
781 value is proportional to the number of replicates of the sample with that score.



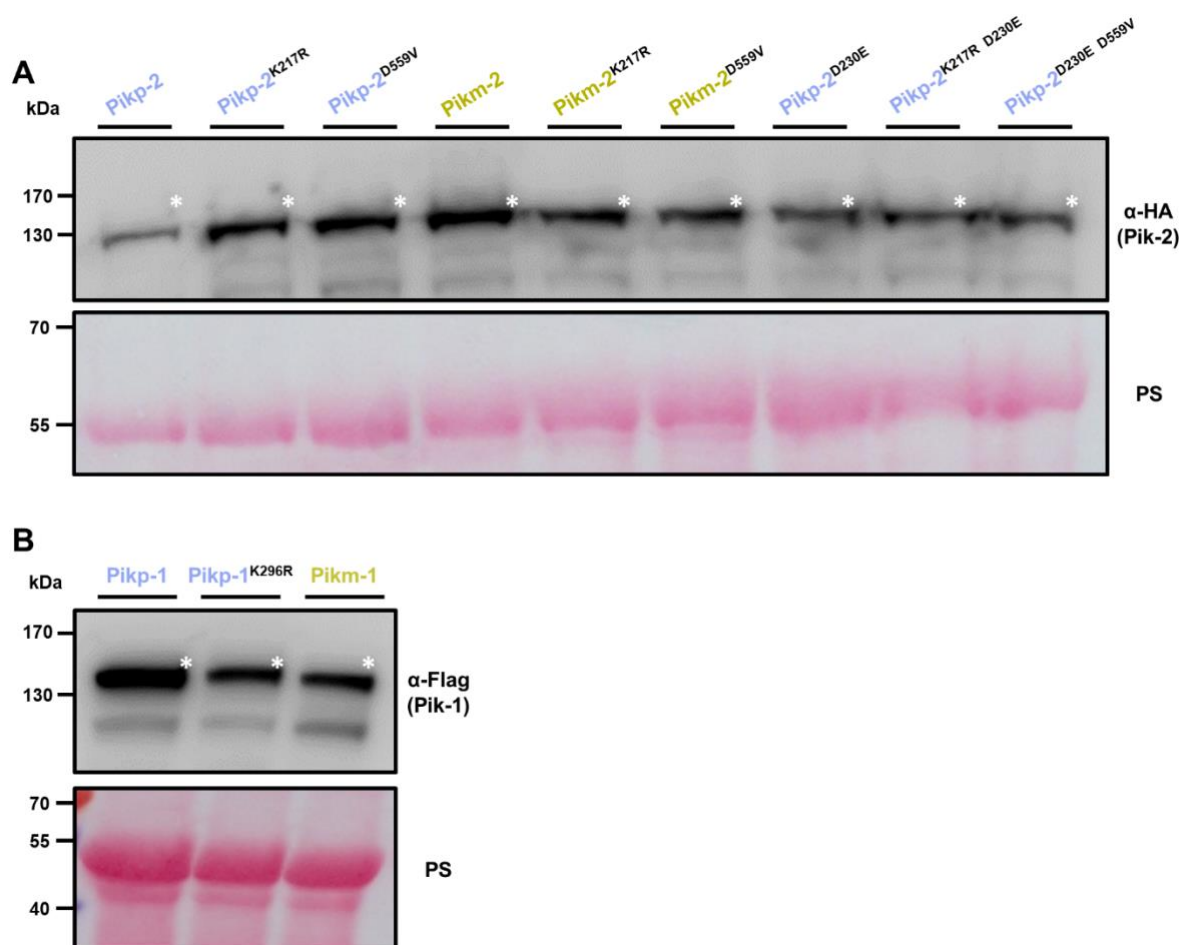
782

783 **Figure S9. Pikp-2 Asp230Glu autoactivation is dependent on P-loop and MHD**  
784 **motifs.** Representative leaf spot images and scoring of Pikm-2 mediated cell death as  
785 autofluorescence under UV-light. Cell death scoring is represented as dot plots  
786 comparing cell death triggered by Pikp-2 Asp230Glu mutant and its versions mutated  
787 in P-loop (Lys217Arg) and MHD (Asp559Val) motifs. Pik-2 mutants were co-  
788 expressed with Pikp-1 and mCherry (red panel) or AVR-PikD (green panel). The  
789 number of repeats was 60 and 30 for the spots co-infiltrated with mCherry and AVR-  
790 PikD, respectively. For each sample, all the data points are represented as dots with a  
791 distinct colour for each of the three biological replicates; these dots are jittered about  
792 the cell death score for visualisation purposes. The size of the central dot at each cell  
793 death value is proportional to the number of replicates of the sample with that score.



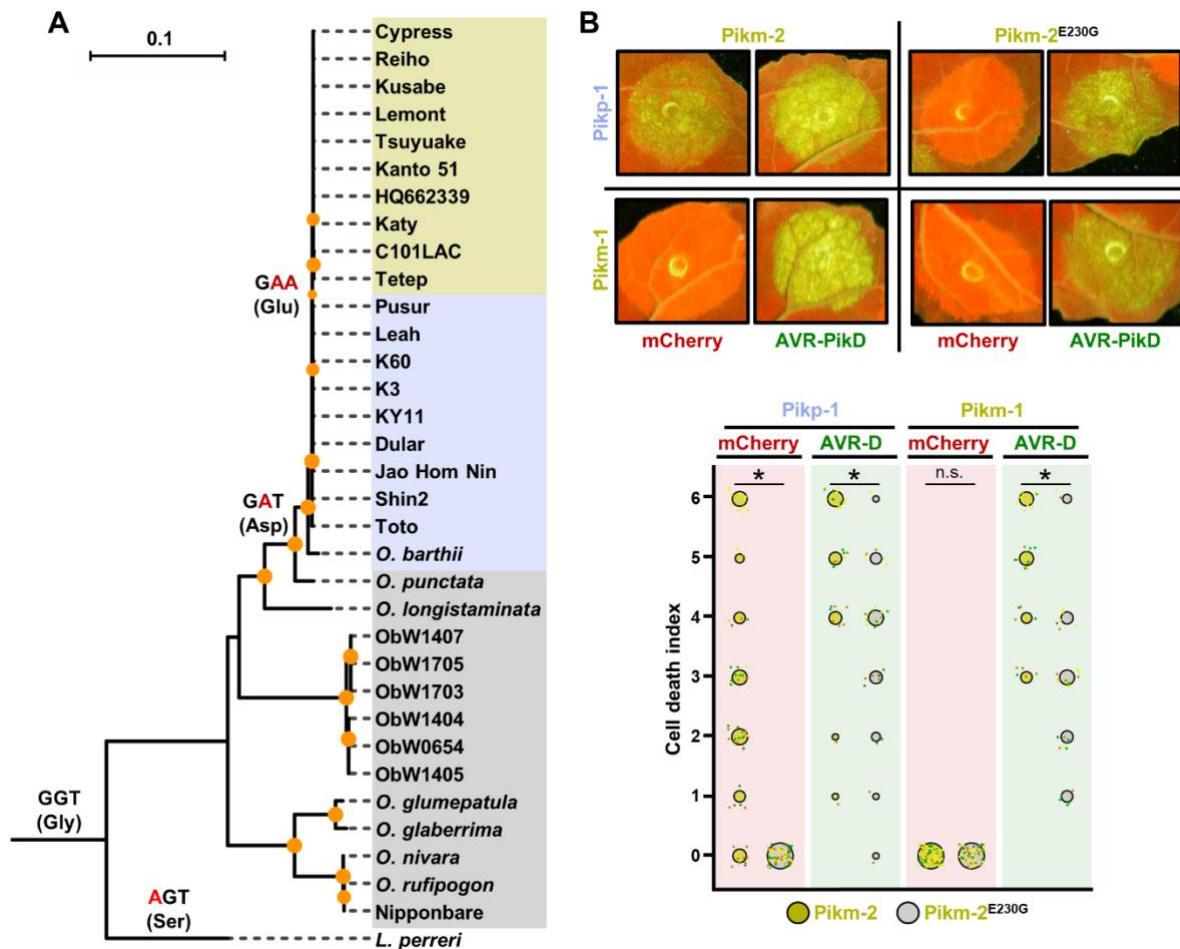
794

795 **Figure S10. The Pik-1 P-loop motif is important but not essential for Pik-mediated**  
 796 **cell death.** Representative leaf spot images and scoring of Pik-mediated cell death as  
 797 autofluorescence under UV-light. Cell death scoring is represented as dot plots  
 798 comparing cell death triggered by Pikm-2 or Pikp-2 Asp230Glu in the presence of  
 799 wild-type Pikp-1 or a version mutated in the P-loop motif (Lys296Arg). The different  
 800 NLR pair combinations were co-infiltrated with mCherry (red panel) or AVR-PikD  
 801 (green panel). The number of repeats was 60 and 30 for the spots co-infiltrated with  
 802 mCherry and AVR-PikD, respectively. For each sample, all the data points are  
 803 represented as dots with a distinct colour for each of the three biological replicates;  
 804 these dots are jittered about the cell death score for visualisation purposes. The size of  
 805 the central dot at each cell death value is proportional to the number of replicates of  
 806 the sample with that score.



807

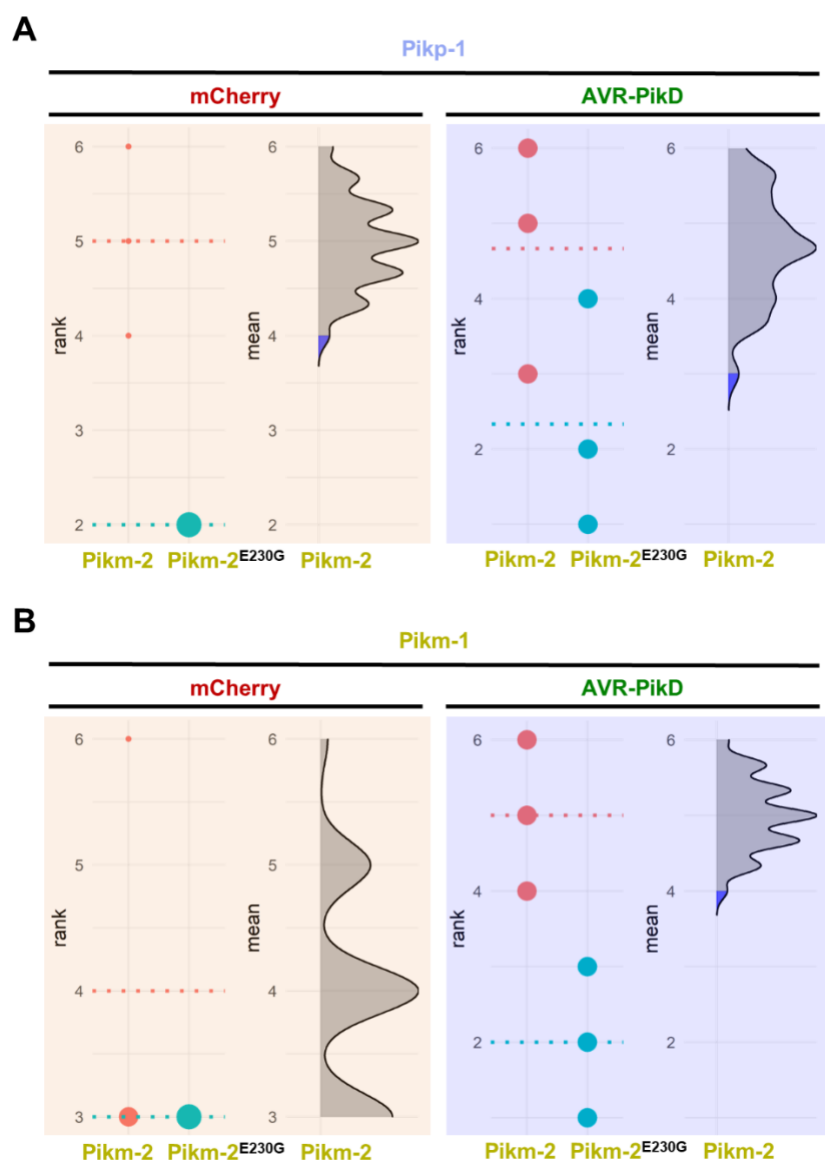
808 **Figure S11. Mutations in P-loop and MHD motifs do not affect protein**  
809 **accumulation.** Western blots showing accumulation of (A) P-loop (Lys217R) and  
810 MHD (Asp559Val) mutants in the background of Pikp-2, Pikm-2 and Pikp-2  
811 Asp230Glu. C-terminally 6×HA tagged Pik-2 mutants were transiently expressed *N.*  
812 *benthamiana*. C-terminally 6×HA tagged Pikp-2, Pikm-2 and Pikp-2 Asp230Glu are  
813 included as controls in each case. (B) Pikp-1 P-loop (Lys296R) mutant. C-terminally  
814 6×His3×FLAG tagged Pikp-1 Lys296Arg mutant was transiently expressed *N.*  
815 *benthamiana*. C-terminally 6×His3×FLAG tagged wild-type Pikp-1 and Pikm-1 are  
816 included as controls (left and right, respectively). Total protein extracts were probed  
817 α-HA and α-FLAG antisera for A and B, respectively. Asterisks mark the band  
818 corresponding to the relevant protein. Total protein loading is shown by Ponceau  
819 staining (PS).



820

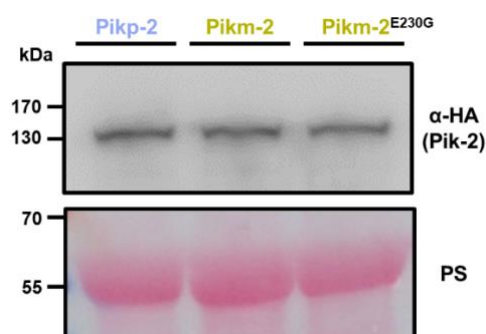
821 **Figure 6. (A) Reconstruction of the evolutionary history of Pik-2 polymorphism at**  
 822 **position 230.** Maximum likelihood (ML) phylogenetic tree of Pik-2 coding sequences  
 823 from cultivated rice and wild rice species. The tree was calculated from a 3,066-nt-long  
 824 alignment using RAxML v8.2.11 (Stamatakis, 2014), 1000 bootstrap method  
 825 (Felsenstein, 1985) and GTRGAMMA substitution model (Tavaré, 1986). Best-scoring  
 826 ML tree was manually rooted using the Pik-2 sequence from *Leersia perreri* as an  
 827 outgroup. The bootstrap values above 80 are indicated with orange circles at the base  
 828 of respective clades; the support values for the relevant nodes are depicted by the size  
 829 of the circle. The scale bar indicates the evolutionary distance based on the nucleotide  
 830 substitution rate. The tree was represented using Interactive Tree Of Life (iTOL) v4  
 831 (Letunic and Bork, 2019). The tree shows a set of inferred nucleotides (states) at the  
 832 Pik-2 polymorphic position 230 based on their predicted likelihood at sites 709 to 711  
 833 of the sequence alignment. Non-synonymous changes at the codon are depicted in red  
 834 next to their corresponding node. For visualization, rice species and cultivars names

835 are shaded in gold, light blue or grey according to their residue in Pik-2 polymorphic  
836 position 230 (Glu, Asp or Gly, respectively). Ob: *Oryza brachyantha*. **(B) Reversion to**  
837 **ancestral state of Pikm-2 Glu230 abolish autoimmunity.** Representative leaf spot  
838 images depicting Pik-mediated cell death as autofluorescence under UV-light in the  
839 presence or absence of AVR-Pik effector. Scoring of the cell death triggered by Pikm-  
840 2 or Pikm-2 Glu230Gly mutant when co-expressed with Pikp-1 or Pikm-1 is  
841 represented as dot plots. The number of repeats was 60 and 30 for the spots co-  
842 infiltrated with mCherry and AVR-PikD, respectively. For each sample, all the data  
843 points are represented as dots with a distinct colour for each of the three biological  
844 replicates; these dots are jittered about the cell death score for visualisation purposes.  
845 The size of the central dot at each cell death value is proportional to the number of  
846 replicates of the sample with that score. Significant differences between relevant  
847 conditions are marked with an asterisk and the details of the statistical analysis are  
848 summarised in **Figure S12**.



849

850 **Figure S12. Estimation graphics for comparison of cell death mediated by Pikm-2**  
851 **or Pikm-2 Glu230Gly.** Statistical analysis by estimation methods of the cell-death  
852 assay for **(A)** Pikp-1 or **(B)** Pikm-1 co-expressed with Pikm-2 Glu230Gly and mCherry  
853 or AVR-PikD, compared with wild-type Pikm-2. The panel on the left represents the  
854 ranked data (dots) for each NLR, and their corresponding mean (dotted line). The size  
855 of the dots is proportional to the number of observations with that specific value. The  
856 panel on the right shows the distribution of 1000 bootstrap sample rank means for Pik-  
857 1 paired with Pikm-2. The blue areas represent the 0.025 and 0.975 percentiles of the  
858 distribution. Pikm-2 Glu230Gly mediated responses are considered significantly  
859 different if the Pikm-2 rank mean (dotted line, left panel) falls beyond the blue regions  
860 of the Pikm-2 Glu230Gly mean distribution.



861

862 **Figure S13. Glu230Gly mutation does not affect Pik-2 protein accumulation.**

863 Western blots showing accumulation of Pikm-2 Glu230Gly. C-terminally 6×HA

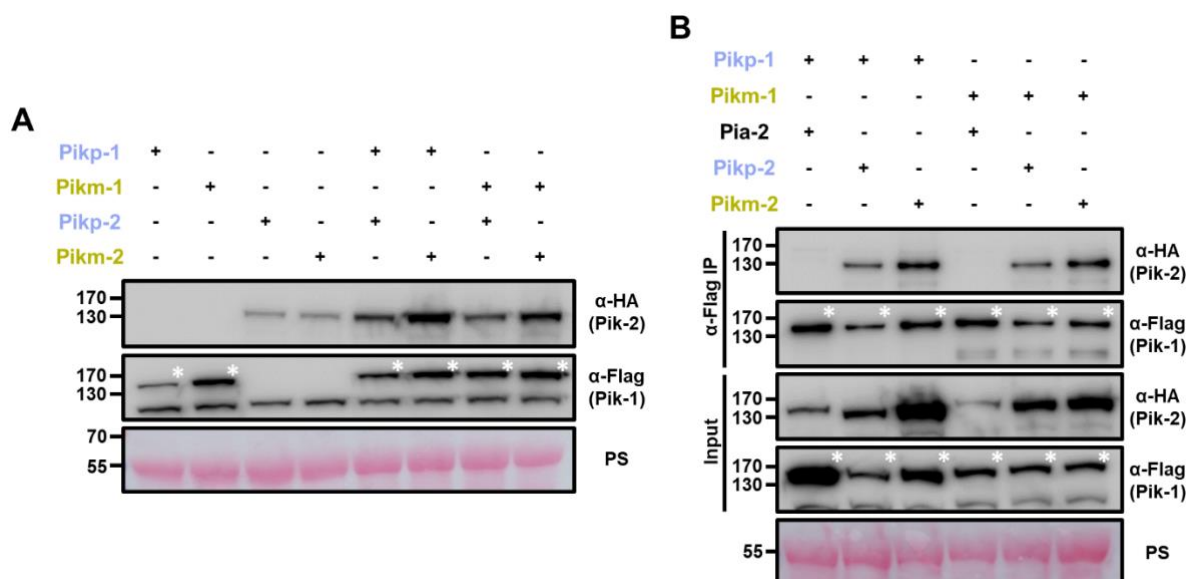
864 tagged Pikm-2 Glu230Gly mutant was transiently expressed *N. benthamiana*. C-

865 terminally 6×HA tagged Pikp-2 and Pikm-2 alleles are included as controls. Total

866 protein extracts were probed α-HA antisera. Total protein loading is shown by

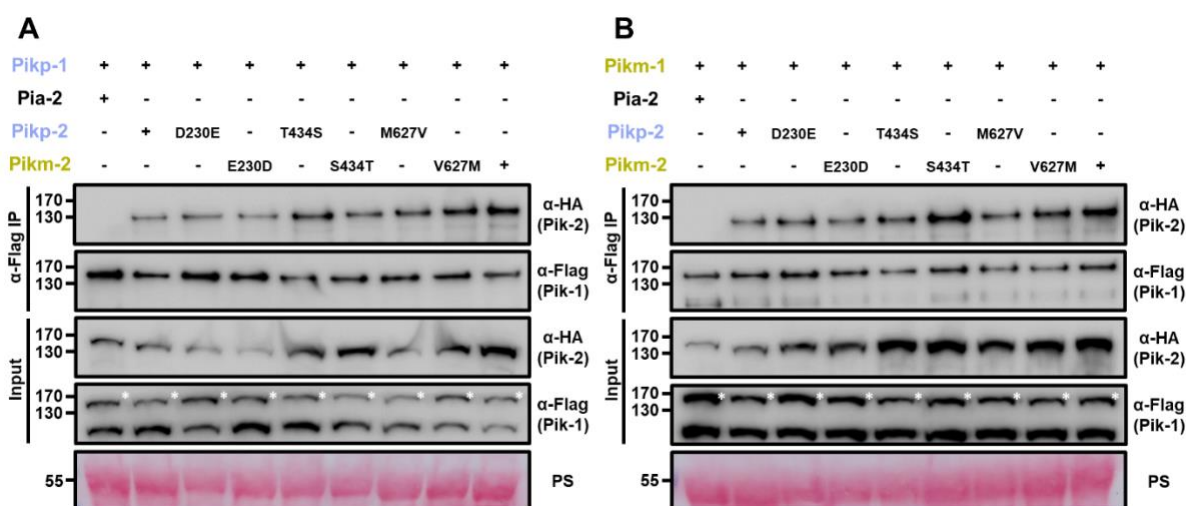
867 Ponceau staining (PS).





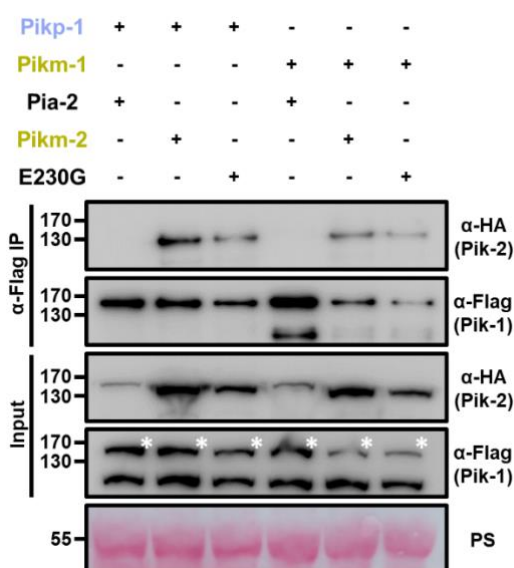
868

869 **Figure 7. (A) Increased protein accumulation of paired Pik proteins when co-**  
870 **expressed together in planta.** Western blots showing protein accumulation of Pik-1  
871 and Pik-2 alleles in different combinations. C-terminally 6×His3×FLAG tagged Pik-1  
872 alleles were transiently co-expressed with empty vector (EV) or C-terminally 6×HA  
873 tagged Pik-2 alleles in *N. benthamiana*. Total protein extracts were probed with α-  
874 FLAG and α-HA antisera for Pik-1 and Pik-2, respectively. Asterisks mark the band  
875 corresponding to Pik-1. **(B) Mismatched Pik NLR pairs associate in planta.** Co-  
876 immunoprecipitation of full-length Pikp-1 and Pikm-1 alleles in combination with  
877 either Pikp-2 or Pikm-2 helper NLRs. C-terminally 6×HA tagged Pia-2, Pikp-2 or  
878 Pikm-2 NLRs were transiently co-expressed with Pikp-1:6×His3×FLAG or Pikm-  
879 1:6×His3×FLAG in *N. benthamiana*. Immunoprecipitates obtained with anti-FLAG  
880 antiserum, and total protein extracts, were probed with appropriate antisera.  
881 Asterisks mark the band corresponding to Pik-1. Total protein loading is shown by  
882 Ponceau staining (PS).



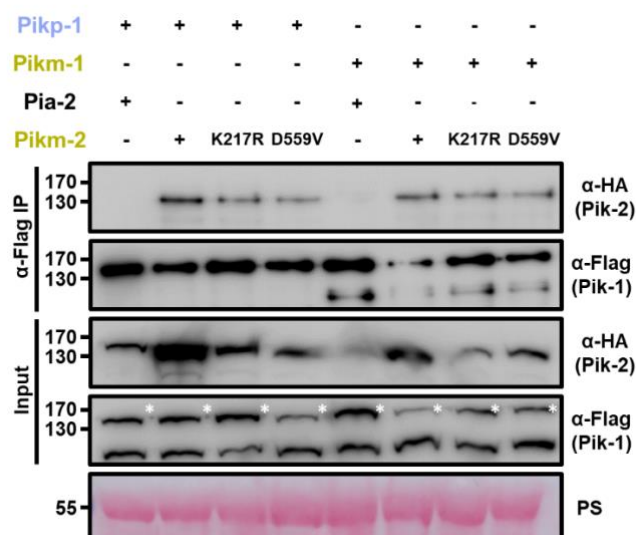
883

884 **Figure S14. Pik-2 mutants associate with Pik-1 in planta.** Co-immunoprecipitation of  
885 full length Pikp-1 (A) or Pikm-1 (B) with each Pik-2 mutant in polymorphic sites. C-  
886 terminally 6×HA tagged Pik-2 NLR mutants were transiently co-expressed with Pik-  
887 1:6×His3×FLAG in *N. benthamiana*. Immunoprecipitates obtained with anti-FLAG  
888 antiserum, and total protein extracts, were probed with appropriate antisera. Co-  
889 expression with C-terminally tagged 6×HA Pia-2 NLR is included as negative control.  
890 Asterisks mark the band corresponding to Pikp-1. Total protein loading is shown by  
891 Ponceau staining (PS).



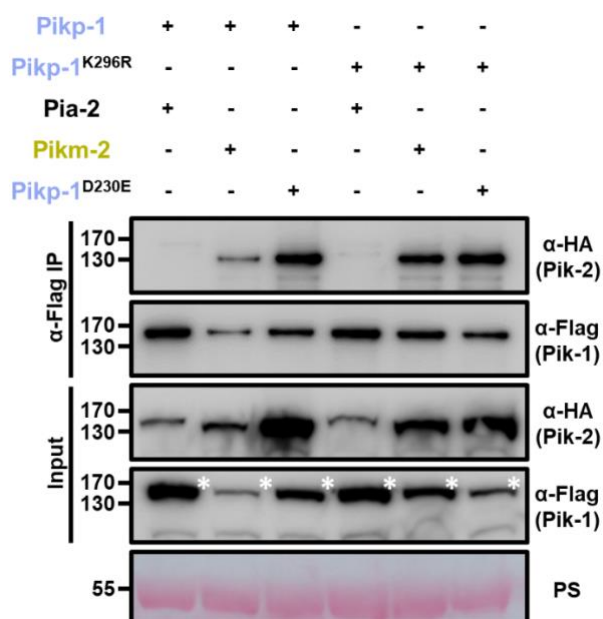
892

893 **Figure S15. Reversion to ancestral state in polymorphism 230 does not abrogate**  
 894 **association with Pik-1 alleles.** Co-immunoprecipitation of Pikm-2 Glu230Gly mutant  
 895 with full length Pikp-1 and Pikm-1 alleles. C-terminally 6×HA tagged Pikm-2  
 896 Glu230Gly was transiently co-expressed with either Pikp-1:6×His3×FLAG or Pikm-  
 897 1:6×His3×FLAG in *N. benthamiana*. Immunoprecipitates obtained with anti-FLAG  
 898 antiserum, and total protein extracts, were probed with appropriate antisera. Co-  
 899 expression with C-terminally tagged 6×HA Pia-2 NLR and wild-type Pikm-2 were  
 900 included as negative and positive control, respectively. Asterisks mark the band  
 901 corresponding to Pik-1. Total protein loading is shown by Ponceau staining (PS).



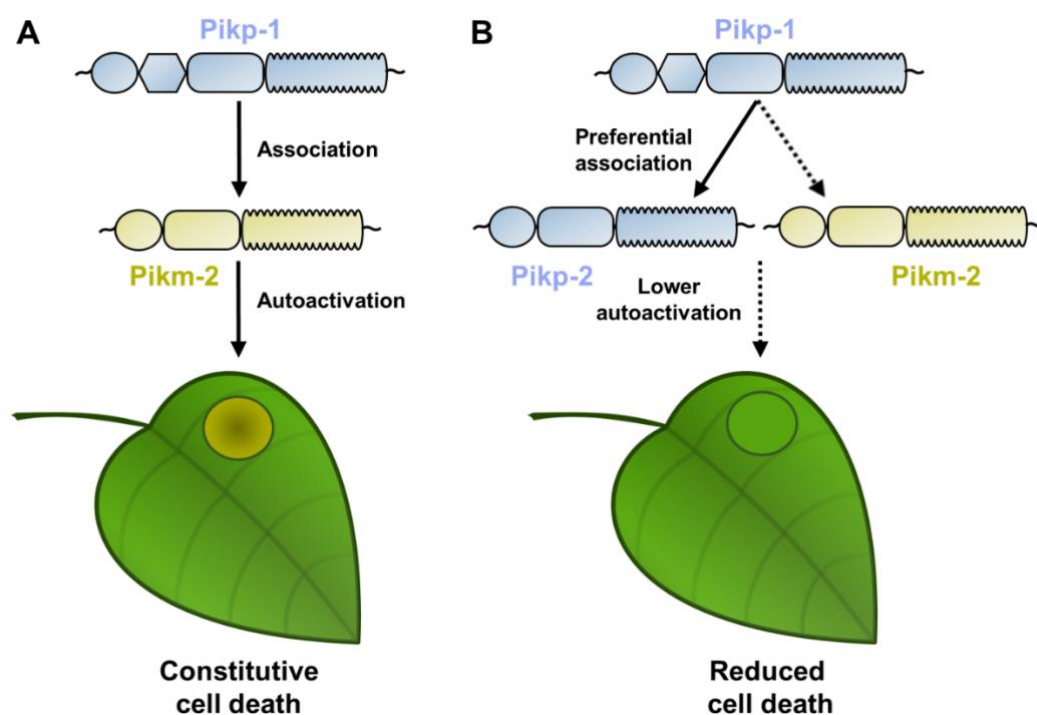
902

903 **Figure 8. Mutations in Pik-2 P-loop and MHD motifs do not affect in planta**  
 904 **association of Pik-1.** Co-immunoprecipitation of Pikm-2 P-loop and MHD mutants  
 905 with full length Pikp-1 and Pikm-1 alleles. C-terminally 6xHA tagged Pikm-2 mutants  
 906 in P-loop (Lys217Arg) and MHD (Asp559Val) motifs were transiently co-expressed  
 907 with either Pikp-1:6xHis3xFLAG or Pikm-1:6xHis3xFLAG in *N. benthamiana*.  
 908 Immunoprecipitates obtained with anti-FLAG antiserum, and total protein extracts,  
 909 were probed with appropriate antisera. Co-expression with C-terminally tagged  
 910 6xHA Pia-2 NLR and wild-type Pikm-2 were included as negative and positive  
 911 control, respectively. Asterisks mark the band corresponding to Pik-1. Total protein  
 912 loading is shown by Ponceau staining (PS).



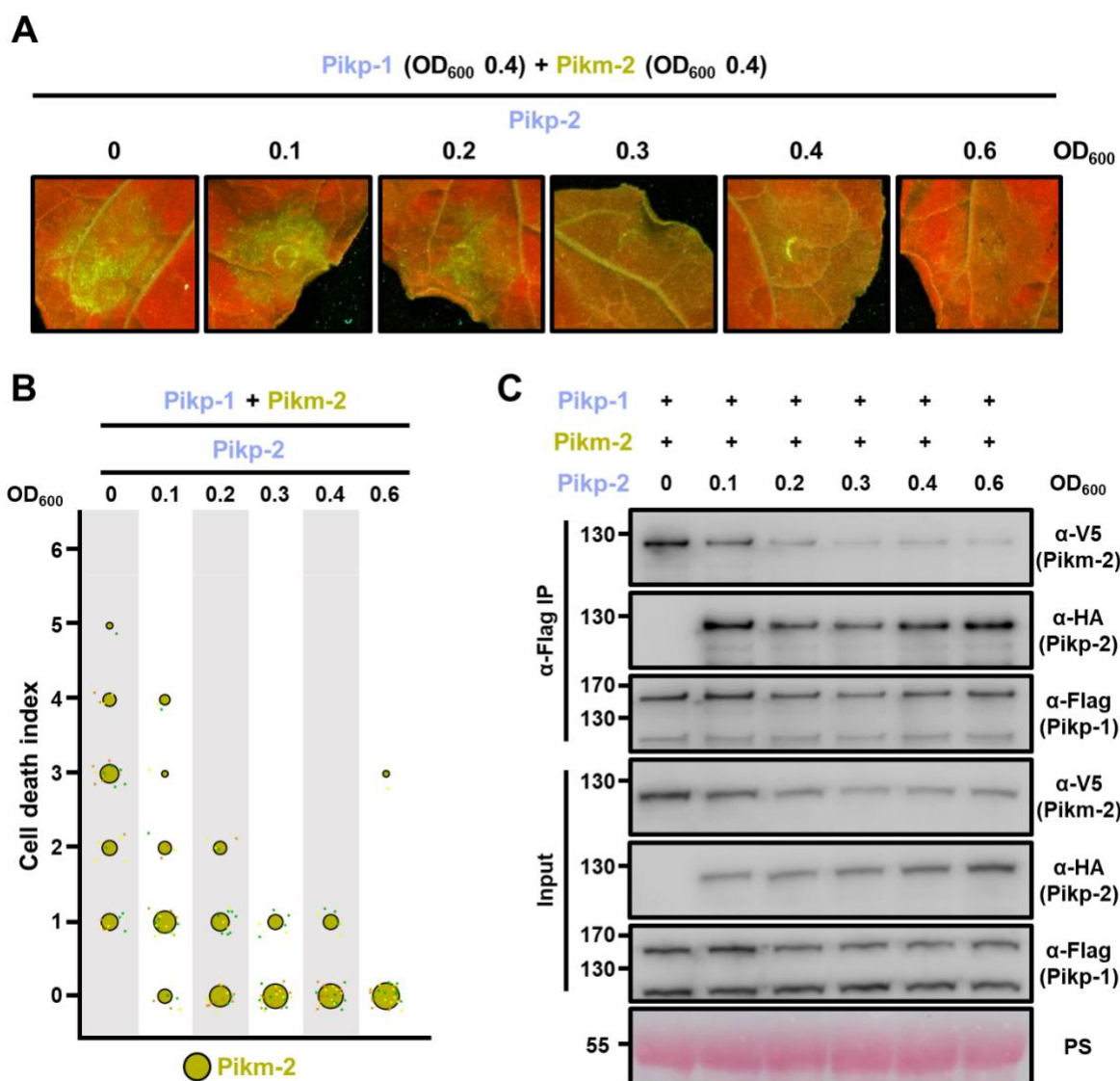
913

914 **Figure S16. P-loop mutations does not affect Pik-1 association to Pik-2.** Co-  
 915 immunoprecipitation of Pikm-2 and Pikp-2 Asp230Glu with wild-type Pikp-1 and  
 916 Pikp-1 P-loop mutant (Lys296Arg). C-terminally 6×HA tagged Pikm-2 and Pikp-2  
 917 Asp230Glu were transiently co-expressed with C-terminally 6×His3×FLAG tagged  
 918 wild-type Pikp-1 or Pikp-1 Lys296Arg in *N. benthamiana*. Immunoprecipitates  
 919 obtained with anti-FLAG antiserum, and total protein extracts, were probed with  
 920 appropriate antisera. Co-expression with C-terminally tagged 6×HA Pia-2 NLR was  
 921 included as negative control, respectively. Asterisks mark the band corresponding to  
 922 Pik-1. Total protein loading is shown by Ponceau staining (PS).



923

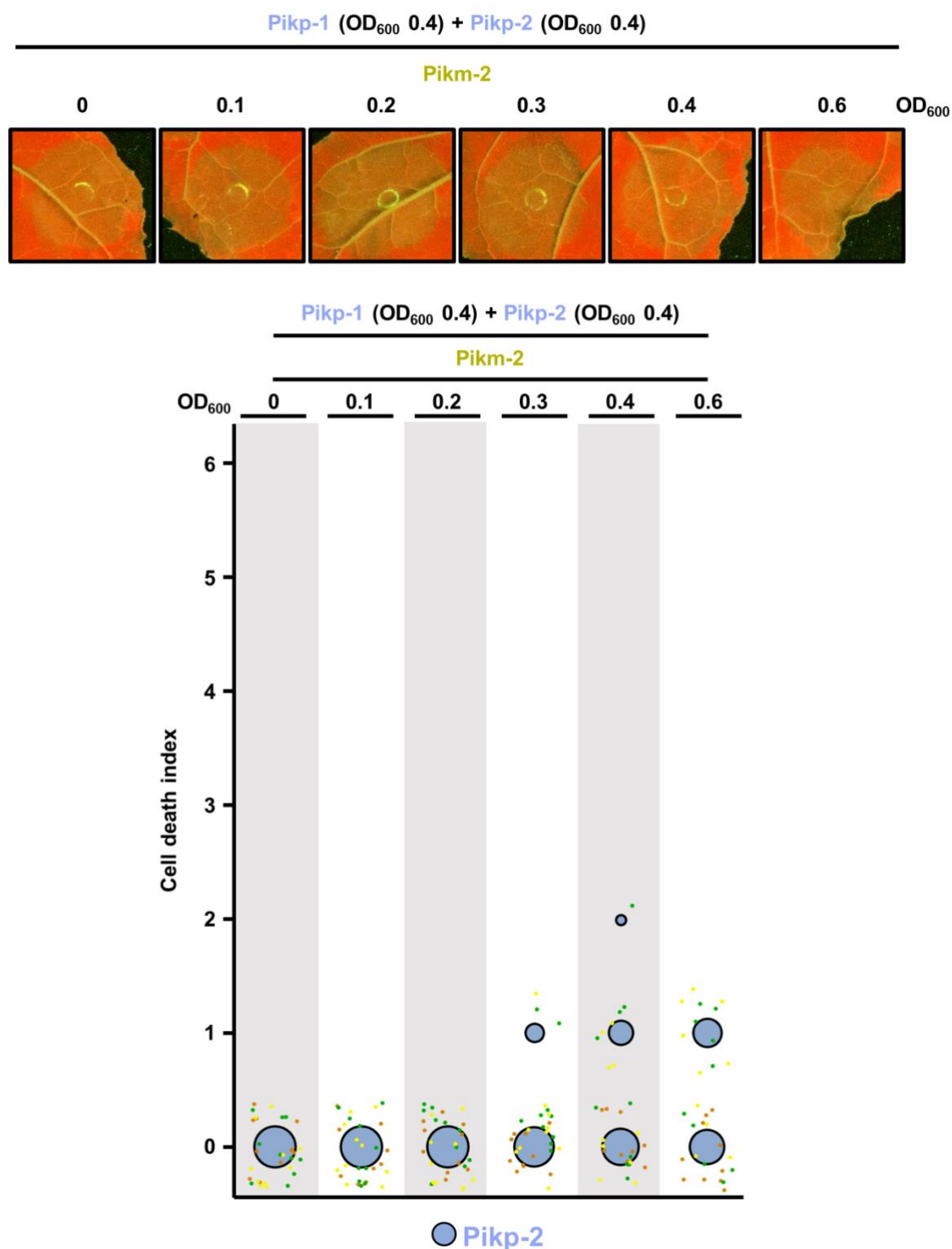
924 **Figure S17. Schematic representations of Pik NLR competition assays. (A)** When  
925 Pikp-1 (coloured in ice blue) is co-expressed with Pikm-2 (coloured in gold), both  
926 NLRs associate and trigger NLR activation that leads to constitutive cell death in *N.*  
927 *benthamiana*, depicted by the development of chlorotic and necrotic leaf tissue. **(B)** In  
928 a preferential association scenario, with both Pikp-2 and Pikm-2 present, Pikp-1 would  
929 associate with coevolved Pikp-2 instead of to Pikm-2 (depicted by the solid and  
930 dashed lines, respectively). This would reduce constitutive immune signalling and cell  
931 death.



932  
 933 **Figure 9. Pikp-2 suppresses constitutive cell death mediated by Pikm-2. (A)**  
 934 Representative leaf spot images depicting Pikm-2 mediated cell death in the presence  
 935 of Pikp-1 and increasing concentration of Pikp-2 as autofluorescence under UV-light.  
 936 For each experiment, Pikp-1 and Pikm-2 were co-infiltrated at OD<sub>600</sub> 0.4 each.  
 937 Increasing concentrations of Pikp-2 were added to each experiment (from left to right:  
 938 OD<sub>600</sub> 0, 0.1, 0.2, 0.3, 0.4 and 0.6). **(B)** Scoring of the cell death assay is represented as  
 939 dot plots. A total of three biological replicates with 10 internal repeats each were  
 940 performed for each experiment. For each sample, all the data points are represented  
 941 as dots with a distinct colour for each of the two biological replicates; these dots are  
 942 jittered about the cell death score for visualisation purposes. The size of the central dot  
 943 at each cell death value is proportional to the number of replicates of the sample with

944 that score. **(C) Pikip-2 outcompetes Pikm-2 association to Pikip-1.** Co-  
945 immunoprecipitation of Pikm-2 and Pikip-1 in the presence of increasing  
946 concentrations on Pikip-2. C-terminally V5 tagged Pikm-2 and C-terminally  
947 6xHis3xFLAG tagged Pikip-1 were transiently co-expressed in *N. benthamiana*  
948 alongside with increasing concentrations of C-terminally 6xHA tagged Pikip-2 (from  
949 left to right: 0, 0.1, 0.2, 0.3, 0.4 and 0.6 OD<sub>600</sub>). Immunoprecipitates obtained with anti-  
950 FLAG antiserum, and total protein extracts, were probed with appropriate antisera.  
951 Asterisks mark the band corresponding to Pikip-1. Total protein loading is shown by  
952 Ponceau staining (PS).



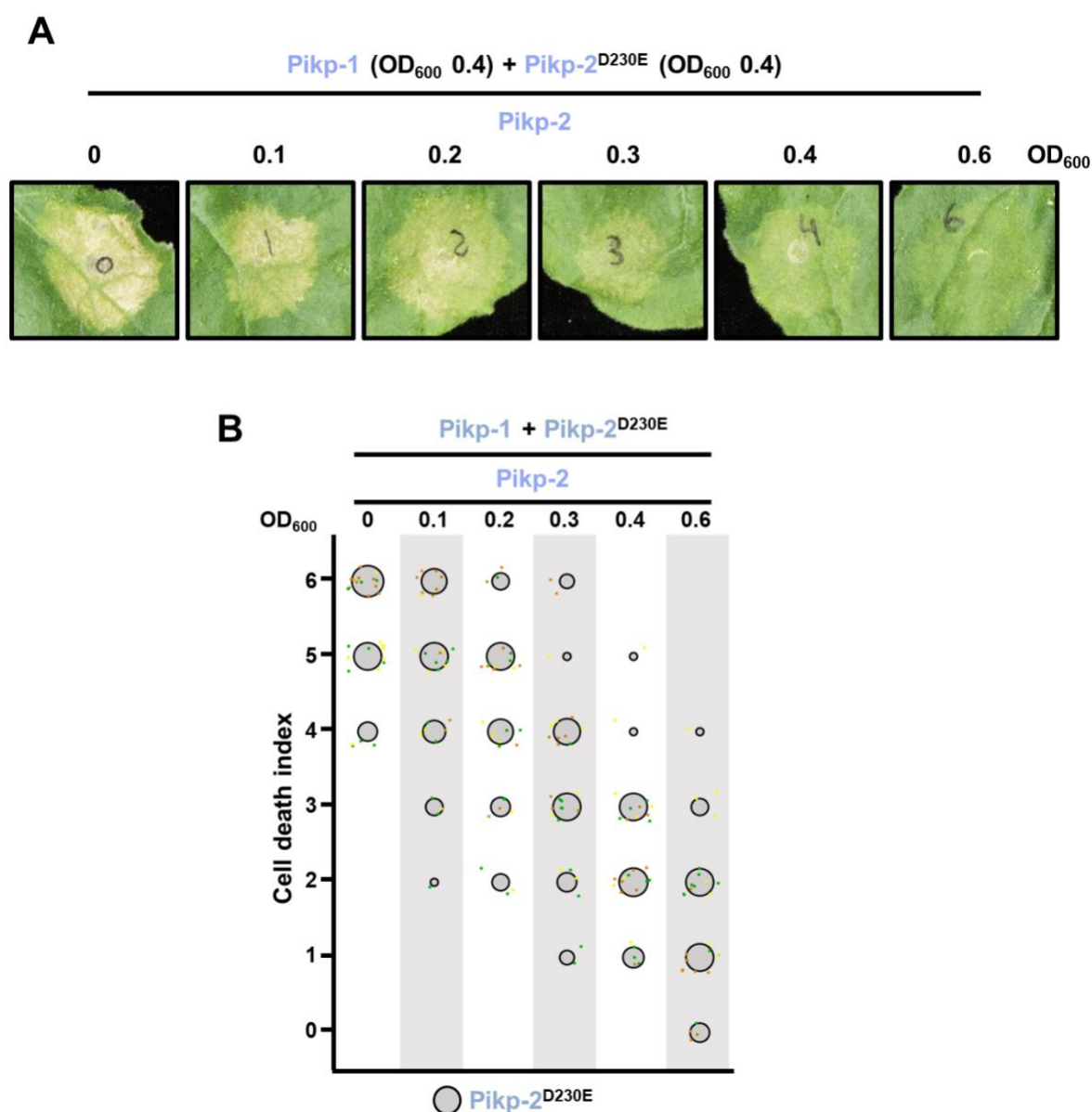


953

954 **Figure S18. Pikp-2 suppresses constitutive cell death mediated by Pikm-2.**

955 Representative leaf spot images depicting Pikm-2 mediated cell death in the presence  
956 of Pikp-1 and Pikp-2 and increasing concentration of Pikm-2 as autofluorescence  
957 under UV-light. Scoring of the cell death assay is represented as dot plots. For each

958 experiment, P<sub>ikp</sub>-1 and P<sub>ikp</sub>-2 were co-infiltrated at OD<sub>600</sub> 0.4 each. Increasing  
959 concentrations of P<sub>ikm</sub>-2 were added to each experiment (from left to right: OD<sub>600</sub> 0,  
960 0.1, 0.2, 0.3, 0.4 and 0.6). A total of three biological replicates with 10 internal repeats  
961 each were performed for each experiment. For each sample, all the data points are  
962 represented as dots with a distinct colour for each of the three biological replicates;  
963 these dots are jittered about the cell death score for visualisation purposes. The size of  
964 the central dot at each cell death value is proportional to the number of replicates of  
965 the sample with that score.



966

967 **Figure 10. Wild-type Pikp-2 suppresses constitutive cell death mediated by Pikp-2**

968 **Asp230Glu mutant. (A)** Representative leaf spot images depicting Pikp-2 Asp230Glu

969 mediated cell death in the presence of Pikp-1 and increasing concentration of Pikp-2.

970 For each experiment, Pikp-1 and Pikp-2 Asp230Glu were co-infiltrated at OD<sub>600</sub> 0.4

971 each. Increasing concentrations of Pikp-2 were added to each experiment (from left to

972 right: OD<sub>600</sub> 0, 0.1, 0.2, 0.3, 0.4 and 0.6). **(B)** Scoring of the cell death mediated by Pikp-

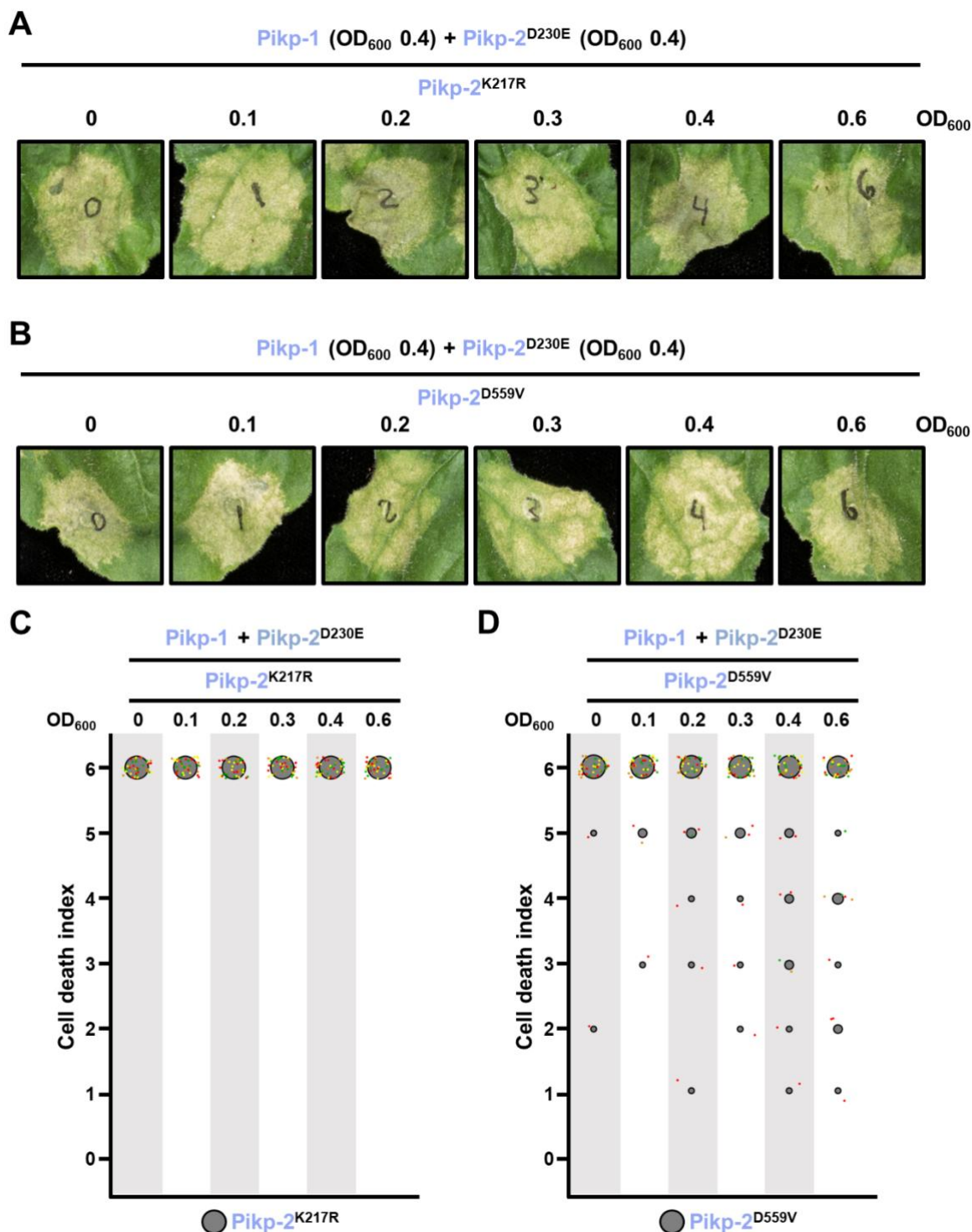
973 2 Asp230Glu in the presence of Pikp-1 and increasing concentration of Pikp-2 assay

974 represented as dot plots. For each experiment, Pikp-1 and Pikp-2 Asp230Glu were co-

975 infiltrated at OD<sub>600</sub> 0.4 each. Increased concentration of Pikp-2 was added to each

976 experiment (from left to right: OD<sub>600</sub> 0, 0.1, 0.2, 0.3, 0.4 and 0.6). A total of three

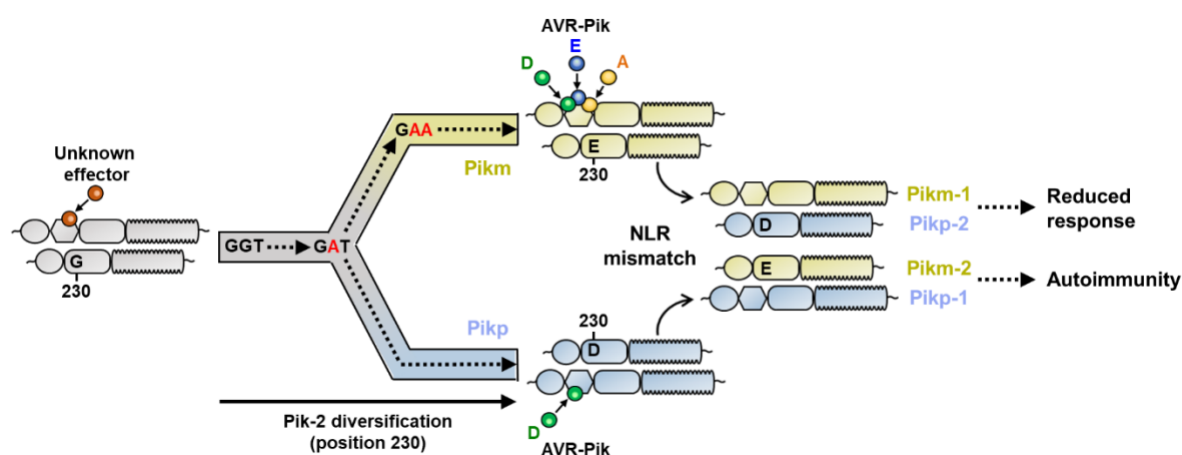
977 biological replicates with 10 internal repeats each were performed for each  
978 experiment. For each sample, all the data points are represented as dots with a distinct  
979 colour for each of the three biological replicates; these dots are jittered about the cell  
980 death score for visualisation purposes. The size of the central dot at each cell death  
981 value is proportional to the number of replicates of the sample with that score.



982

983 **Figure 11. Suppression of constitutive cell death mediated by Pikp-2 Asp230Glu**  
 984 **requires an active Pikp-2.** Representative leaf spot images depicting Pikp-2  
 985 Asp230Glu mediated cell death in the presence of Pikp-1 and increasing concentration  
 986 of Pikp-2. For each experiment, Pikp-1 and Pikp-2 Asp230Glu were co-infiltrated at  
 987 OD<sub>600</sub> 0.4 each. Increasing concentrations of **(A)** Pikp-2 Lys217Arg or **(B)** Pikp-2

988 Asp559Val were added to each experiment (from left to right: OD<sub>600</sub> 0, 0.1, 0.2, 0.3, 0.4  
989 and 0.6). Scoring of the cell death mediated by P<sub>ikp</sub>-2 Asp230Glu in the presence of  
990 P<sub>ikp</sub>-1 and increasing concentration of **(C)** P<sub>ikp</sub>-2 Lys217Arg or **(D)** P<sub>ikp</sub>-2 Asp559Val  
991 represented as dot plots. For each experiment, P<sub>ikp</sub>-1 and P<sub>ikp</sub>-2 Asp230Glu were co-  
992 infiltrated at OD<sub>600</sub> 0.4 each. Increased concentration of P<sub>ikp</sub>-2 mutants were added to  
993 each experiment (from left to right: OD<sub>600</sub> 0, 0.1, 0.2, 0.3, 0.4 and 0.6). A total of four  
994 biological replicates with 10 internal repeats each were performed for each  
995 experiment. For each sample, all the data points are represented as dots with a distinct  
996 colour for each of the four biological replicates; these dots are jittered about the cell  
997 death score for visualisation purposes. The size of the central dot at each cell death  
998 value is proportional to the number of replicates of the sample with that score.



999

1000 **Figure 12. Schematic representation of the proposed evolutionary model of the Pik**  
 1001 **pairing.** Pikp (coloured in ice blue) and Pikm (coloured in gold), have evolved and  
 1002 specialized from an ancestral NLR pair (coloured in grey), functionally diversifying  
 1003 and gaining recognition to a different subset of allelic AVR-Pik effectors. Residues at  
 1004 Pik-2 polymorphic position 230 are indicated and mutations predicted to have  
 1005 occurred during this transition are indicated in red. As a consequence of  
 1006 diversification, mismatch of Pikp and Pikm impairs immune responses and leads to  
 1007 NLR autoactivation and constitutive cell death in *N. benthamiana*.

## 1008 **References**

1009

1010 Adachi, H., Contreras, M., Harant, A., Wu, C.-h., Derevnina, L., Sakai, T., Duggan, C., Moratto, E.,  
1011 Bozkurt, T.O., Maqbool, A., *et al.* (2019a). An N-terminal motif in NLR immune receptors is functionally  
1012 conserved across distantly related plant species. *bioRxiv*, 693291.

1013 Adachi, H., Derevnina, L., and Kamoun, S. (2019b). NLR singletons, pairs, and networks: evolution,  
1014 assembly, and regulation of the intracellular immunoreceptor circuitry of plants. *Current Opinion in*  
1015 *Plant Biology* 50, 121-131.

1016 Ashikawa, I., Hayashi, N., Yamane, H., Kanamori, H., Wu, J., Matsumoto, T., Ono, K., and Yano, M.  
1017 (2008). Two adjacent nucleotide-binding site-leucine-rich repeat class genes are required to confer  
1018 Pikm-specific rice blast resistance. *Genetics* 180, 2267-2276.

1019 Bailey, P.C., Schudoma, C., Jackson, W., Baggs, E., Dagdas, G., Haerty, W., Moscou, M., and Krasileva,  
1020 K.V. (2018). Dominant integration locus drives continuous diversification of plant immune receptors  
1021 with exogenous domain fusions. *Genome Biol* 19, 23.

1022 Barragan, A.C., and Weigel, D. (2020). Plant NLR Diversity: The Known Unknowns of Pan-NLRomes.  
1023 *The Plant cell*.

1024 Barragan, C.A., Wu, R., Kim, S.T., Xi, W., Habring, A., Hagmann, J., Van de Weyer, A.L., Zaidem, M., Ho,  
1025 W.W.H., Wang, G., *et al.* (2019). RPW8/HR repeats control NLR activation in *Arabidopsis thaliana*. *PLoS*  
1026 *genetics* 15, e1008313.

1027 Bentham, A.R., De la Concepcion, J.C., Mukhi, N., Zdrzalek, R., Draeger, M., Gorenkin, D., Hughes, R.K.,  
1028 and Banfield, M.J. (2020). A molecular roadmap to the plant immune system. *J Biol Chem*.

1029 Bentham, A.R., Petit-Houdenot, Y., Win, J., Chuma, I., Terauchi, R., Banfield, M.J., Kamoun, S., and  
1030 Langner, T. (2021). A single amino acid polymorphism in a conserved effector of the multihost blast  
1031 fungus pathogen expands host-target binding spectrum. *bioRxiv*, 2021.2003.2015.435478.

1032 Bernoux, M., Burdett, H., Williams, S.J., Zhang, X., Chen, C., Newell, K., Lawrence, G.J., Kobe, B., Ellis,  
1033 J.G., Anderson, P.A., *et al.* (2016). Comparative Analysis of the Flax Immune Receptors L6 and L7  
1034 Suggests an Equilibrium-Based Switch Activation Model. *The Plant cell* 28, 146-159.

1035 Bialas, A., Langner, T., Harant, A., Contreras, M.P., Stevenson, C.E.M., Lawson, D.M., Sklenar, J.,  
1036 Kellner, R., Moscou, M.J., Terauchi, R., *et al.* (2021). Two NLR immune receptors acquired high-affinity  
1037 binding to a fungal effector through convergent evolution of their integrated domain. *bioRxiv*,  
1038 2021.2001.2026.428286.

1039 Bialas, A., Zess, E.K., De la Concepcion, J.C., Franceschetti, M., Pennington, H.G., Yoshida, K., Upson,  
1040 J.L., Chanclud, E., Wu, C.H., Langner, T., *et al.* (2018). Lessons in Effector and NLR Biology of Plant-  
1041 Microbe Systems. *Mol Plant Microbe Interact* 31, 34-45.

1042 Bomblies, K., Lempe, J., Epple, P., Warthmann, N., Lanz, C., Dangl, J.L., and Weigel, D. (2007).  
1043 Autoimmune response as a mechanism for a Dobzhansky-Muller-type incompatibility syndrome in  
1044 plants. *PLoS Biol* 5, e236.

1045 Bomblies, K., and Weigel, D. (2007). Hybrid necrosis: autoimmunity as a potential gene-flow barrier in  
1046 plant species. *Nat Rev Genet* 8, 382-393.

1047 Caldwell, R.M., and Compton, L.E. (1943). COMPLEMENTARY LETHAL GENES IN WHEAT: Causing a  
1048 Progressive Lethal Necrosis of Seedlings\*. *Journal of Heredity* 34, 67-70.

1049 Calvo-Baltanás, V., Wang, J., and Chae, E. (2021). Hybrid Incompatibility of the Plant Immune System:  
1050 An Opposite Force to Heterosis Equilibrating Hybrid Performances. *Frontiers in Plant Science* 11.

1051 Cesari, S., Bernoux, M., Moncuquet, P., Kroj, T., and Dodds, P.N. (2014a). A novel conserved  
1052 mechanism for plant NLR protein pairs: the "integrated decoy" hypothesis. *Front Plant Sci* 5, 606.

1053 Cesari, S., Kanzaki, H., Fujiwara, T., Bernoux, M., Chalvon, V., Kawano, Y., Shimamoto, K., Dodds, P.,  
1054 Terauchi, R., and Kroj, T. (2014b). The NB-LRR proteins RGA4 and RGA5 interact functionally and  
1055 physically to confer disease resistance. *EMBO J* 33, 1941-1959.

1056 Cesari, S., Thilliez, G., Ribot, C., Chalvon, V., Michel, C., Jauneau, A., Rivas, S., Alaux, L., Kanzaki, H.,  
1057 Okuyama, Y., *et al.* (2013). The rice resistance protein pair RGA4/RGA5 recognizes the *Magnaporthe*  
1058 *oryzae* effectors AVR-Pia and AVR1-CO39 by direct binding. *The Plant cell* 25, 1463-1481.



- 1059 Chae, E., Bomblies, K., Kim, S.T., Karelina, D., Zaidem, M., Ossowski, S., Martin-Pizarro, C., Laitinen,  
1060 R.A., Rowan, B.A., Tenenboim, H., *et al.* (2014). Species-wide genetic incompatibility analysis identifies  
1061 immune genes as hot spots of deleterious epistasis. *Cell* *159*, 1341-1351.
- 1062 Chae, E., Tran, D.T., and Weigel, D. (2016). Cooperation and Conflict in the Plant Immune System. *PLoS*  
1063 *Pathog* *12*, e1005452.
- 1064 Chaipanya, C., Telebanco-Yanoria, M.J., Quime, B., Longya, A., Korinsak, S., Korinsak, S., Toojinda, T.,  
1065 Vanavichit, A., Jantasuriyarat, C., and Zhou, B. (2017). Dissection of broad-spectrum resistance of the  
1066 Thai rice variety Jao Hom Nin conferred by two resistance genes against rice blast. *Rice (N Y)* *10*, 18-  
1067 18.
- 1068 Costanzo, S., and Jia, Y. (2010). Sequence variation at the rice blast resistance gene Pi-km locus:  
1069 Implications for the development of allele specific markers. *Plant Science* *178*, 523-530.
- 1070 De la Concepcion, J.C., Franceschetti, M., MacLean, D., Terauchi, R., Kamoun, S., and Banfield, M.J.  
1071 (2019). Protein engineering expands the effector recognition profile of a rice NLR immune receptor.  
1072 *eLife* *8*, e47713.
- 1073 De la Concepcion, J.C., Franceschetti, M., Maqbool, A., Saitoh, H., Terauchi, R., Kamoun, S., and  
1074 Banfield, M.J. (2018). Polymorphic residues in rice NLRs expand binding and response to effectors of  
1075 the blast pathogen. *Nat Plants* *4*, 576-585.
- 1076 De la Concepcion, J.C., Maidment, J.H.R., Longya, A., Xiao, G., Franceschetti, M., and Banfield, M.J.  
1077 (2021). The allelic rice immune receptor Pikh confers extended resistance to strains of the blast fungus  
1078 through a single polymorphism in the effector binding interface. *PLOS Pathogens* *17*, e1009368.
- 1079 Dobzhansky, T. (1937). *GENETICS AND THE ORIGIN OF SPECIES*. Columbia Univ Press, New York.
- 1080 Edgar, R.C. (2004). MUSCLE: multiple sequence alignment with high accuracy and high throughput.  
1081 *Nucleic Acids Res* *32*, 1792-1797.
- 1082 Eitas, T.K., and Dangl, J.L. (2010). NB-LRR proteins: pairs, pieces, perception, partners, and pathways.  
1083 *Curr Opin Plant Biol* *13*, 472-477.
- 1084 Engler, C., Youles, M., Gruetzner, R., Ehnert, T.M., Werner, S., Jones, J.D., Patron, N.J., and Marillonnet,  
1085 S. (2014). A golden gate modular cloning toolbox for plants. *ACS Synth Biol* *3*, 839-843.
- 1086 Felsenstein, J. (1985). Confidence Limits on Phylogenies: An Approach Using the Bootstrap. *Evolution*  
1087 *39*, 783-791.
- 1088 Griebel, T., Maekawa, T., and Parker, J.E. (2014). NOD-like receptor cooperativity in effector-triggered  
1089 immunity. *Trends in Immunology* *35*, 562-570.
- 1090 Hermesen, J.G.T. (1963a). The genetic basis of hybrid necrosis in wheat. *Genetica* *33*, 245-287.
- 1091 Hermesen, J.G.T. (1963b). Hybrid necrosis as a problem for the wheat breeder. *Euphytica* *12*, 1-16.
- 1092 Hu, Z., Zhou, Q., Zhang, C., Fan, S., Cheng, W., Zhao, Y., Shao, F., Wang, H.-W., Sui, S.-F., and Chai, J.  
1093 (2015). Structural and biochemical basis for induced self-propagation of NLRC4. *Science* *350*, 399-404.
- 1094 Hua, L., Wu, J., Chen, C., Wu, W., He, X., Lin, F., Wang, L., Ashikawa, I., Matsumoto, T., Wang, L., *et al.*  
1095 (2012). The isolation of Pi1, an allele at the Pik locus which confers broad spectrum resistance to rice  
1096 blast. *TAG Theoretical and applied genetics Theoretische und angewandte Genetik* *125*, 1047-1055.
- 1097 Hurni, S., Brunner, S., Stirnweis, D., Herren, G., Peditto, D., McIntosh, R.A., and Keller, B. (2014). The  
1098 powdery mildew resistance gene Pm8 derived from rye is suppressed by its wheat ortholog Pm3. *Plant*  
1099 *J* *79*, 904-913.
- 1100 Jones, J.D.G., Vance, R.E., and Dangl, J.L. (2016). Intracellular innate immune surveillance devices in  
1101 plants and animals. *Science* *354*, aaf6395.
- 1102 Jubic, L.M., Saile, S., Furzer, O.J., El Kasmi, F., and Dangl, J.L. (2019). Help wanted: helper NLRs and  
1103 plant immune responses. *Current Opinion in Plant Biology* *50*, 82-94.
- 1104 Kanzaki, H., Yoshida, K., Saitoh, H., Fujisaki, K., Hirabuchi, A., Alaux, L., Fournier, E., Tharreau, D., and  
1105 Terauchi, R. (2012). Arms race co-evolution of *Magnaporthe oryzae* AVR-Pik and rice Pik genes driven  
1106 by their physical interactions. *Plant J* *72*, 894-907.
- 1107 Karasov, T.L., Chae, E., Herman, J.J., and Bergelson, J. (2017). Mechanisms to Mitigate the Trade-Off  
1108 between Growth and Defense. *The Plant cell* *29*, 666-680.

- 1109 Kiyosawa, S. (1969). INHERITANCE OF BLAST-RESISTANCE IN WEST PAKISTANI RICE VARIETY, PUSUR.  
1110 Japanese Journal of Breeding 19, 121-128.
- 1111 Kiyosawa, S. (1978). Identification of Blast-Resistance Genes in Some Rice Varieties. Japanese Journal  
1112 of Breeding 28, 287-296.
- 1113 Klose, K.E., Weiss, D.S., and Kustu, S. (1993). Glutamate at the Site of Phosphorylation of Nitrogen-  
1114 regulatory Protein NTRC Mimics Aspartyl-Phosphate and Activates the Protein. Journal of molecular  
1115 biology 232, 67-78.
- 1116 Kourelis, J., Sakai, T., Adachi, H., and Kamoun, S. (2021). RefPlantNLR: a comprehensive collection of  
1117 experimentally validated plant NLRs. bioRxiv, 2020.2007.2008.193961.
- 1118 Kroj, T., Chanclud, E., Michel-Romiti, C., Grand, X., and Morel, J.B. (2016). Integration of decoy domains  
1119 derived from protein targets of pathogen effectors into plant immune receptors is widespread. New  
1120 Phytol 210, 618-626.
- 1121 Le Roux, C., Huet, G., Jauneau, A., Camborde, L., Tremousaygue, D., Kraut, A., Zhou, B., Levallant, M.,  
1122 Adachi, H., Yoshioka, H., *et al.* (2015). A receptor pair with an integrated decoy converts pathogen  
1123 disabling of transcription factors to immunity. Cell 161, 1074-1088.
- 1124 Letunic, I., and Bork, P. (2019). Interactive Tree Of Life (iTOL) v4: recent updates and new  
1125 developments. Nucleic Acids Research 47, W256-W259.
- 1126 Li, L., Habring, A., Wang, K., and Weigel, D. (2020). Atypical Resistance Protein RPW8/HR Triggers  
1127 Oligomerization of the NLR Immune Receptor RPP7 and Autoimmunity. Cell Host Microbe 27, 405-  
1128 417.e406.
- 1129 Li, L., and Weigel, D. (2021). One Hundred Years of Hybrid Necrosis: Hybrid Autoimmunity as a Window  
1130 into the Mechanisms and Evolution of Plant-Pathogen Interactions. Annu Rev Phytopathol.
- 1131 Ma, S., Lapin, D., Liu, L., Sun, Y., Song, W., Zhang, X., Logemann, E., Yu, D., Wang, J., Jirschitzka, J., *et*  
1132 *al.* (2020). Direct pathogen-induced assembly of an NLR immune receptor complex to form a  
1133 holoenzyme. Science 370, eabe3069.
- 1134 Maidment, J.H.R., Franceschetti, M., Maqbool, A., Saitoh, H., Jantasuriyarat, C., Kamoun, S., Terauchi,  
1135 R., and Banfield, M.J. (2021). Multiple variants of the fungal effector AVR-Pik bind the HMA domain of  
1136 the rice protein OsHIPP19, providing a foundation to engineer plant defence. J Biol Chem, 100371.
- 1137 Maqbool, A., Saitoh, H., Franceschetti, M., Stevenson, C.E., Uemura, A., Kanzaki, H., Kamoun, S.,  
1138 Terauchi, R., and Banfield, M.J. (2015). Structural basis of pathogen recognition by an integrated HMA  
1139 domain in a plant NLR immune receptor. Elife 4.
- 1140 Martin, R., Qi, T., Zhang, H., Liu, F., King, M., Toth, C., Nogales, E., and Staskawicz, B.J. (2020). Structure  
1141 of the activated ROQ1 resistosome directly recognizing the pathogen effector XopQ. Science 370,  
1142 eabd9993.
- 1143 Meyers, B.C., Kozik, A., Griego, A., Kuang, H., and Michelmore, R.W. (2003). Genome-wide analysis of  
1144 NBS-LRR-encoding genes in Arabidopsis. The Plant cell 15, 809-834.
- 1145 Oikawa, K., Fujisaki, K., Shimizu, M., Takeda, T., Saitoh, H., Hirabuchi, A., Hiraka, Y., Białas, A., Langner,  
1146 T., Kellner, R., *et al.* (2020). The blast pathogen effector AVR-Pik binds and stabilizes rice heavy metal-  
1147 associated (HMA) proteins to co-opt their function in immunity. bioRxiv, 2020.2012.2001.406389.
- 1148 Pupko, T., Pe'er, I., Shamir, R., and Graur, D. (2000). A fast algorithm for joint reconstruction of  
1149 ancestral amino acid sequences. Mol Biol Evol 17, 890-896.
- 1150 Richard, M.M.S., and Takken, F.L.W. (2017). Plant Autoimmunity: When Good Things Go Bad. Curr Biol  
1151 27, R361-R363.
- 1152 Sakai, H., Honma, T., Aoyama, T., Sato, S., Kato, T., Tabata, S., and Oka, A. (2001). ARR1, a Transcription  
1153 Factor for Genes Immediately Responsive to Cytokinins. Science 294, 1519-1521.
- 1154 Sarris, P.F., Cevik, V., Dagdas, G., Jones, J.D., and Krasileva, K.V. (2016). Comparative analysis of plant  
1155 immune receptor architectures uncovers host proteins likely targeted by pathogens. BMC Biol 14, 8.
- 1156 Sarris, P.F., Duxbury, Z., Huh, S.U., Ma, Y., Segonzac, C., Sklenar, J., Derbyshire, P., Cevik, V., Rallapalli,  
1157 G., Saucet, S.B., *et al.* (2015). A Plant Immune Receptor Detects Pathogen Effectors that Target WRKY  
1158 Transcription Factors. Cell 161, 1089-1100.

- 1159 Saur, I.M.L., Panstruga, R., and Schulze-Lefert, P. (2020). NOD-like receptor-mediated plant immunity:  
1160 from structure to cell death. *Nature Reviews Immunology*.
- 1161 Sharif, H., Wang, L., Wang, W.L., Magupalli, V.G., Andreeva, L., Qiao, Q., Hauenstein, A.V., Wu, Z.,  
1162 Nunez, G., Mao, Y., *et al.* (2019). Structural mechanism for NEK7-licensed activation of NLRP3  
1163 inflammasome. *Nature* **570**, 338-343.
- 1164 Stamatakis, A. (2014). RAxML version 8: a tool for phylogenetic analysis and post-analysis of large  
1165 phylogenies. *Bioinformatics* **30**, 1312-1313.
- 1166 Stein, J.C., Yu, Y., Copetti, D., Zwickl, D.J., Zhang, L., Zhang, C., Chougule, K., Gao, D., Iwata, A.,  
1167 Goicoechea, J.L., *et al.* (2018). Genomes of 13 domesticated and wild rice relatives highlight genetic  
1168 conservation, turnover and innovation across the genus *Oryza*. *Nature Genetics* **50**, 285-296.
- 1169 Stirnweis, D., Milani, S.D., Brunner, S., Herren, G., Buchmann, G., Peditto, D., Jordan, T., and Keller, B.  
1170 (2014). Suppression among alleles encoding nucleotide-binding-leucine-rich repeat resistance  
1171 proteins interferes with resistance in F1 hybrid and allele-pyramided wheat plants. *The Plant Journal*  
1172 **79**, 893-903.
- 1173 Tameling, W.I., Elzinga, S.D., Darmin, P.S., Vossen, J.H., Takken, F.L., Haring, M.A., and Cornelissen, B.J.  
1174 (2002). The tomato R gene products I-2 and MI-1 are functional ATP binding proteins with ATPase  
1175 activity. *The Plant cell* **14**, 2929-2939.
- 1176 Tameling, W.I.L., Vossen, J.H., Albrecht, M., Lengauer, T., Berden, J.A., Haring, M.A., Cornelissen, B.J.C.,  
1177 and Takken, F.L.W. (2006). Mutations in the NB-ARC domain of I-2 that impair ATP hydrolysis cause  
1178 autoactivation. *Plant physiology* **140**, 1233-1245.
- 1179 Tavaré, S. (1986). Some probabilistic and statistical problems in the analysis of DNA sequences.
- 1180 Tenthorey, J.L., Haloupek, N., López-Blanco, J.R., Grob, P., Adamson, E., Hartenian, E., Lind, N.A.,  
1181 Bourgeois, N.M., Chacón, P., Nogales, E., *et al.* (2017). The structural basis of flagellin detection by  
1182 NAIP5: A strategy to limit pathogen immune evasion. *Science* **358**, 888-893.
- 1183 To, J.P.C., Deruère, J., Maxwell, B.B., Morris, V.F., Hutchison, C.E., Ferreira, F.J., Schaller, G.E., and  
1184 Kieber, J.J. (2007). Cytokinin Regulates Type-A Arabidopsis Response Regulator Activity and Protein  
1185 Stability via Two-Component Phosphorelay. *The Plant cell* **19**, 3901-3914.
- 1186 Tran, D.T.N., Chung, E.H., Habring-Muller, A., Demar, M., Schwab, R., Dangl, J.L., Weigel, D., and Chae,  
1187 E. (2017). Activation of a Plant NLR Complex through Heteromeric Association with an Autoimmune  
1188 Risk Variant of Another NLR. *Curr Biol* **27**, 1148-1160.
- 1189 Van de Weyer, A.-L., Monteiro, F., Furzer, O.J., Nishimura, M.T., Cevik, V., Witek, K., Jones, J.D.G.,  
1190 Dangl, J.L., Weigel, D., and Bemm, F. (2019). A Species-Wide Inventory of NLR Genes and Alleles in  
1191 *Arabidopsis thaliana*. *Cell* **178**, 1260-1272.e1214.
- 1192 Wan, W.-L., Kim, S.-T., Castel, B., Charoennit, N., and Chae, E. (2021). Genetics of autoimmunity in  
1193 plants: an evolutionary genetics perspective. *New Phytologist* **229**, 1215-1233.
- 1194 Wang, J., Hu, M., Wang, J., Qi, J., Han, Z., Wang, G., Qi, Y., Wang, H.-W., Zhou, J.-M., and Chai, J.  
1195 (2019a). Reconstitution and structure of a plant NLR resistosome conferring immunity. *Science* **364**,  
1196 eaav5870.
- 1197 Wang, J., Wang, J., Hu, M., Wu, S., Qi, J., Wang, G., Han, Z., Qi, Y., Gao, N., Wang, H.-W., *et al.* (2019b).  
1198 Ligand-triggered allosteric ADP release primes a plant NLR complex. *Science* **364**, eaav5868.
- 1199 Wang, L., Zhao, L., Zhang, X., Zhang, Q., Jia, Y., Wang, G., Li, S., Tian, D., Li, W.-H., and Yang, S. (2019c).  
1200 Large-scale identification and functional analysis of *NLR* genes in blast resistance in the  
1201 Tetep rice genome sequence. *Proceedings of the National Academy of Sciences*, 201910229.
- 1202 Wickham, H. (2016). *ggplot2: Elegant Graphics for Data Analysis* (Springer-Verlag New York).
- 1203 Williams, S.J., Sornaraj, P., deCourcy-Ireland, E., Menz, R.I., Kobe, B., Ellis, J.G., Dodds, P.N., and  
1204 Anderson, P.A. (2011). An autoactive mutant of the M flax rust resistance protein has a preference for  
1205 binding ATP, whereas wild-type M protein binds ADP. *Mol Plant Microbe Interact* **24**, 897-906.
- 1206 Win, J., Chaparro-Garcia, A., Belhaj, K., Saunders, D.G., Yoshida, K., Dong, S., Schornack, S., Zipfel, C.,  
1207 Robatzek, S., Hogenhout, S.A., *et al.* (2012). Effector biology of plant-associated organisms: concepts  
1208 and perspectives. *Cold Spring Harb Symp Quant Biol* **77**, 235-247.

- 1209 Wu, C.-H., Derevnina, L., and Kamoun, S. (2018). Receptor networks underpin plant immunity. *Science*  
1210 *360*, 1300-1301.
- 1211 Xu, X., Hayashi, N., Wang, C.T., Kato, H., Fujimura, T., and Kawasaki, S. (2008). Efficient authentic fine  
1212 mapping of the rice blast resistance gene *Pik-h* in the *Pik* cluster, using new *Pik-h*-differentiating  
1213 isolates. *Molecular Breeding* *22*, 289-299.
- 1214 Yamamoto, E., Takashi, T., Morinaka, Y., Lin, S., Wu, J., Matsumoto, T., Kitano, H., Matsuoka, M., and  
1215 Ashikari, M. (2010). Gain of deleterious function causes an autoimmune response and Bateson-  
1216 Dobzhansky-Muller incompatibility in rice. *Molecular genetics and genomics : MGG* *283*, 305-315.
- 1217 Yang, Z. (1997). PAML: a program package for phylogenetic analysis by maximum likelihood. *Comput*  
1218 *Appl Biosci* *13*, 555-556.
- 1219 Yang, Z., Kumar, S., and Nei, M. (1995). A new method of inference of ancestral nucleotide and amino  
1220 acid sequences. *Genetics* *141*, 1641-1650.
- 1221 Yoshida, K., Saitoh, H., Fujisawa, S., Kanzaki, H., Matsumura, H., Yoshida, K., Tosa, Y., Chuma, I., Takano,  
1222 Y., Win, J., *et al.* (2009). Association genetics reveals three novel avirulence genes from the rice blast  
1223 fungal pathogen *Magnaporthe oryzae*. *The Plant cell* *21*, 1573-1591.
- 1224 Yue, J.X., Meyers, B.C., Chen, J.Q., Tian, D., and Yang, S. (2012). Tracing the origin and evolutionary  
1225 history of plant nucleotide-binding site-leucine-rich repeat (NBS-LRR) genes. *New Phytol* *193*, 1049-  
1226 1063.
- 1227 Zdrzalek, R., Kamoun, S., Terauchi, R., Saitoh, H., and Banfield, M.J. (2020). The rice NLR pair *Pikp-*  
1228 *1/Pikp-2* initiates cell death through receptor cooperation rather than negative regulation. *PloS one*  
1229 *15*.
- 1230 Zhang, L., Chen, S., Ruan, J., Wu, J., Tong, A.B., Yin, Q., Li, Y., David, L., Lu, A., Wang, W.L., *et al.* (2015).  
1231 Cryo-EM structure of the activated NAIP2-NLRC4 inflammasome reveals nucleated polymerization.  
1232 *Science* *350*, 404-409.
- 1233